ROLES OF PARTICLE BREAKAGE AND DRAINAGE IN THE ISOTROPIC COMPRESSION OF SAND TO HIGH PRESSURES

by Woongju Mun, Ph.D., S.M. ASCE[1] and John S. McCartney, Ph.D., P.E., M. ASCE[2]

Abstract: The roles of particle breakage and drainage conditions on the quasi-static compression response of sand were evaluated by comparing the results from drained and undrained isotropic compression tests on dry and saturated specimens up to a mean total stress of 160 MPa. For dry sand specimens, the compression curves from drained and undrained tests were similar due to the high compressibility of air. The isotropic compression curves of the dry sand specimens at mean stresses greater than 30 MPa reflect a transition toward void closure, reaching a minimum void ratio of 0.04 at 160 MPa. Dry sand specimens with different initial relative densities showed similar behavior during isotropic compression in drained conditions for mean stresses greater than approximately 30 MPa. As expected, saturated specimens tested under undrained conditions showed a much stiffer response than in drained conditions, with a bulk modulus greater than that of water. Increasing trends in particle breakage quantified using the breakage factors of Marsal and Hardin with increasing mean stress were observed for the dry sand specimens, but negligible particle breakage was noted for the saturated specimens tested in undrained conditions. To highlight the linkage between particle breakage and the transition to void closure at high mean effective stress, an empirical relationship was developed using Hardin's relative breakage index to match the experimentally-derived compression curves of dry sands under drained conditions.

[1] Senior Staff Engineer, Converse Consultants, 717 South Myrtle Avenue, Monrovia, CA, 91016; woongju.mun@gmail.com
[2] Associate Professor, University of California San Diego, Department of Structural Engineering. 9500 Gilman Dr., La Jolla, CA 92093-0085, mccartney@ucsd.edu.

INTRODUCTION

It is well known that granular materials may experience particle breakage during isotropic or uniaxial compression to high mean effective stresses as well as during subsequent shearing. Of these different stress paths, the particle breakage during isotropic compression has not been as widely studied as during uniaxial (oedometric) compression or shearing, potentially because less particle breakage is expected when shear stresses are not applied. Accordingly, this study focuses on the role of particle breakage in sand during isotropic compression to high mean effective stresses under quasi-static loading rates and different pore fluid drainage conditions. Although some studies have defined different ranges of mean effective stresses at which soil behavior may change (Vesić and Clough 1968; Akers 2001), high mean effective stresses are defined in this study as those greater than typically encountered in geotechnical applications (i.e., 10 MPa). An investigation of particle breakage during isotropic compression to high mean effective stresses is relevant as recent studies have sought to link the particle breakage to transitions in soil behavior during different stress paths (Nakata et al. 2001a, 2001b; McDowell 2002; Einav 2007a; Einav 2007b; Ezaoui et al. 2011; Zhang and Buscarnera 2014). Further, a better understanding of the isotropic compression curve of sands to high stresses will also help improve the prediction of soil response during the detonation of buried explosives. Specifically, many blast simulation models use the parameters of the quasi-static isotropic compression curve as important constitutive inputs, such as the Hybrid-Elastic-Plastic (HEP) constitutive model (Zimmerman et al. 1987; Akers et al. 1995; Moral et al. 2010), even though soils may experience high loading rates and different stress paths during buried explosions. A particular focus of these models is the identification of the transition to void closure at which the no further changes in volume occur with increasing pressure, which may require particle breakage to reach.

This study presents the results from isotropic compression tests on dry and saturated sands to different mean stresses up to 160 MPa to quantify the amount of particle breakage and the role of different drainage conditions on the shape of the isotropic compression curve. The mean effective stress of 160 MPa was selected based on the upper range of the pressure control system employed in the experimental setup, and is much lower than the maximum blast pressure of approximately 3400 MPa expected in buried explosions (Moral et al. 2010). Nonetheless, it is sufficient to detect the initiation of the transition to void closure expected in most soils and to evaluate the evolution of particle breakage with mean effective stress in sands. Although the primary focus of this study was on the drained isotropic compression of dry sand under different initial void ratios, additional tests were performed to assess the role of pore air drainage in dry sands and pore water drainage in saturated sands. In the case of the isotropic compression of saturated sands in drained conditions, the mean effective stress is not expected to change. However, the differences between the compressibility values of the pore fluid and soil skeleton may lead to particle rearrangement and crushing, so it is relevant to confirm if this could lead to particle crushing under high mean stresses. When assessing the different experimental results, the breakage factors defined by Marsal (1967) and Hardin (1985) were used to quantify particle breakage after isotropic compression to different mean stresses.

BACKGROUND

Lessons Learned from Particle Breakage during Shearing

The role of particle breakage in sands during shearing under high mean stresses has been studied by several researchers over the past 60 years (Hall and Gordon 1963; Hirschfield and Poulos 1963; Bishop et al. 1965; Bishop 1966; Lee and Seed 1967; Vesić and Clough 1968; Tai 1970; Murphy 1971; Lo and Roy 1973; Colliat-Dangus et al. 1988; Yamamuro and Lade 1996a; Akers 2001;

66 Salim et al. 2004; Bazazzadeh et al. 2011; Vilhar et al. 2013; Ghafghazi et al. 2014). Although the
67 conditions for particle breakage are different from those encountered during isotropic compression,
68 these studies permit an understanding of the main variables controlling particle breakage. General
69 observations that can be drawn from these studies are that the particle mineralogy and hardness
70 play a major role in the amount of breakage, more particle breakage occurs during shearing as the
71 mean effective stresses increases, and the particle size distribution of poorly graded soils will shift
72 toward a more well-graded condition after shearing. The shift in the particle size distribution,
73 particle breakage is the primary factor that governs changes in the stress-strain behavior and
74 friction angle of granular material as they are sheared under increasingly higher mean effective
75 stresses. Variables that play a role in particle breakage include the initial particle size distribution,
76 particle shape, particle strength, particle mineralogy, particle angularity and the degree of
77 saturation (Hendron et al. 1969; Hagerty et al. 1993; Akers 2001). The initial density of the
78 specimen has less of an effect on particle breakage during shearing high mean stresses (Vesić and
79 Clough 1968), and the uniaxial compression curves of sands having different densities tend to
80 converge at high mean effective stresses above 3 to 30 MPa depending on the sand mineralogy
81 (Hendron 1963; Yamamuro et al. 1996b; Altuhafi and Coop 2011). In addition, the stress path is
82 important, with more particle breakage occurring in specimens having lower degrees of freedom
83 such as plane-strain conditions (Marachi et al. 1969; Becker et al. 1972). Likewise, shearing in
84 drained or undrained conditions may also affect particle breakage due to the constraint on volume
85 change during shearing, but this has not been thoroughly studied. The amount of particle breakage
86 is also a function of the shearing rate, which has been investigated in studies involving either very
87 slow loading (creep) (Schmertmann 1991; Yamamuro and Lade, 1993; Gupta 2000; Oldecop and
88 Alonso 2003) or fast loading (Fukuoka et al 1990; Wang and Yan 2011; Omidvar et al 2012).

Lessons Learned from Particle Breakage during Compression

Although not as widely investigated as in the case of shearing, particle breakage also occurs during isotropic or uniaxial (anisotropic) compression over a wide range of mean effective stresses. The drained compression curve of sands has been characterized in isotropic tests (Lee and Seed 1967; Marachi et al. 1969; Mazanti and Holland 1970; Holland 1971; Murphy 1971; Coop and Lee 1993; Nakata et al. 2001a, 2001b; Vilhar et al. 2013) or uniaxial (oedometer) tests (Hendron 1963; Akers et al. 1986; Golightly 1990; Biarze and Hicher 1994; Hagerty et al. 1993; Coop and Lee 1993; Yamamuro et al. 1996b; Akers 2001; Altuhafi and Coop 2011) to mean effective stresses ranging from 10 to 850 MPa. Several of these studies evaluated particle breakage during compression under these different compression stress paths, and other studies also presented syntheses of particle breakage characteristics from these studies (Fukumoto 1992; Pestana and Whittle 1995; McDowell and Bolton 1998; Akers 2001). Coop and Lee (1993) found that the mean effective stress level at the initiation of measurable particle breakage ranges from 0.1 to 2 MPa, and that the magnitude of this mean effective stress level is related to the individual particle strength. The evolution in particle breakage of sands during uniaxial compression with mean effective stress has been investigated in several studies, who generally observed a greater change in particle breakage with mean effective stress for sands with weaker particles (Fukumoto 1992; Coop and Lee 1993; Hagerty et al. 1993; McDowell and Bolton 1998; Vilhar et al. 2013). Although less particle breakage is observed during isotropic compression than during shear (Coop and Lee, 1993), isotropic compression is an important stress path, and particle breakage is a key mechanism that may contribute to the nonlinearity of the transition in the compression curve toward void closure at high mean effective stresses.

Although many studies have used the conventional bi-log-linear model to capture the virgin compression response of sands (Novello and Johnston, 1989; Been et al. 1991; Pestana et al. 1995; McDowell et al. 1996; Verdugo and Ishihara 1996; Konrad 1998; Russell and Khalili 2002; Muir Wood 2008; Muir Wood and Maeda 2008; Bandini and Coop 2011; Vilhar et al. 2013), many sands exhibit a smooth, highly nonlinear compression curve both during initial yielding as well as at higher mean effective stresses above 20-30 MPa (Golightly 1990; Yamamuro and Lade 1996b). A hypothetical representation of typical uniaxial compression curves of saturated sands with different initial densities compressed to high mean effective stresses is shown in Figure 1, based on observations from Biarez and Hicher (1994) and Yamamuro et al. (1996b). Although it needs to be confirmed if the shapes of the uniaxial compression curves in this figure are also representative of isotropic compression conditions, a discussion of the shapes of the uniaxial compression curves is useful to highlight different transition points in the compression curves. During uniaxial compression of sand from a given initial void ratio, an initial elastic response is typically observed, with a similar slope regardless of the initial sand density (A-B). A nonlinear yielding process is typically observed with increasing mean effective stress and the compression curve will follow a log-linear trend typically referred to as the normal compression line (B-C). At some point on the normal compression line, measurable particle breakage will start to initiate and the shape of the compression curve will eventually start to deviate from the conventional bi-log-linear trend (C). The rearrangement of sand particles along with particle breakage results in an increasingly dense particle arrangement, which leads to an increase in the number and area of contact points between particles. This contributes to a hardening response as particle rearrangement becomes more difficult during the transition to void closure (C-D). At void closure (D), the uniaxial compression curve approaches either a void ratio of zero or a constant small void

ratio, and continued changes in mean effective stress are possible without further changes in void ratio. During unloading after uniaxial compression to high mean effective stresses up to point C, most sands show an elastic, log-linear response if unloaded before the hardening response (E-F). However, during unloading after uniaxial compression beyond the point that hardening starts, Yamamuro et al. (1996b) observed a nonlinear unloading response that transitions to a log-linear response at lower mean effective stresses (E′-F′). Although it appears from the shape of the hypothetical uniaxial unloading line that this response is softer than the unloading response from lower mean stresses, this is due to the plotting of the mean effective stress on a logarithmic plot, as will be discussed later.

The pore fluid drainage conditions may have a major effect on the particle breakage and may contribute to the shape of the compression curve. The uniaxial compression curves for dry sand in undrained conditions (no drainage of pore air), or for saturated sand in undrained conditions (no drainage of pore water) have not been fully assessed. Whitman (1970) observed that the pore fluid phase of water-saturated soils may be stiffer than the soil skeleton due to the low compressibility of water, while the soil skeleton is generally stiffer than the pore fluid phases at lower degrees of saturation S_r (i.e., S_r less than 0.5). The compression response of dry sand in undrained conditions is expected to be similar to the response of dry sand in drained conditions due to the high compressibility of air, but this hasn't been confirmed. Similarly, the compression response of saturated sand in undrained conditions is expected to be much stiffer than the compression response of dry or saturated sand in drained conditions, and as stiff as or stiffer than the compression response of water. Although the effective stress state is not expected to change during isotropic compression of saturated sand in undrained conditions, it is not clear if particle breakage or rearrangement would occur during application of high mean total stresses. The presence of pore

157 water may change the surface energy of the sand particles, which may make water-saturated sand
158 more susceptible to particle breakage than dry sand (Miura and Yamanouchi 1975; Zhang and
159 Buscarnera 2014). This phenomenon is expected to be the most significant for rock fill materials
160 which contain large particles (Leslie 1975) and has been used to explain settlements related with
161 inundation of granular fills for dams (Sowers et al. 1965).

162 Several studies have used devices such as the Split-Hopkinson pressure bar (SPHB) to evaluate
163 the uniaxial compression curve under extremely high stresses as well as high rates (Whitman 1970;
164 Charlie et al. 1990; Veyera 1994; Field et al. 2004; Martin et al. 2009; Kabir et al. 2010; Omidvar
165 et al. 2012; Luo et al. 2015). Although these tests were intended to be performed in uniaxial
166 conditions (Hendron 1963; Richart et al. 1970), it is possible that under the high stresses associated
167 with particle breakage that some lateral expansion of the cell may occur. This may lead to a change
168 in the stress state that affects the shape of the compression curve obtained from these experiments.
169 Most of the studies using the SPHB have observed a strain hardening effect and an S-shaped
170 compression curve. Furthermore, there may be rate effects that prevent characterization of
171 important transition points in the compression curve over the full range of mean effective stress,
172 which can be affected by particle rearrangement, particle breakage, or inter-particle bonding under
173 high contact stresses greater than 20 to 30 MPa (Whitman 1970; Veyera 1994; Omidvar et al.
174 2012). The uniaxial compression response of soils under both dynamic and static loading
175 conditions at various strain rates have been experimentally investigated by several researchers
176 (Farr and Woods 1988; Hendron 1963; Hendron et al. 1969; Whitman et al. 1964; Whitman 1970;
177 Wu et al. 1984). They observed that the uniaxial stress-strain behavior of soils subjected to high
178 intensity transient loading differs from the response measured under static conditions and that rate
179 effects become very critical at sub-millisecond loading times.

After measurement of the compression curve of soils under high stresses, different constitutive relationships can be fitted to the data for use in numerical simulations. The Hybrid-Elastic-Plastic (HEP) constitutive model is formulated to consider both the shear and compression behavior of geologic material during blast loading (Zimmerman et al. 1987; Akers et al. 1995). The HEP model uses a segmental log-linear isotropic compression curve for geological materials that extends up to mean stresses up to 3400 MPa. Akers (2001) also developed a nonlinear hysteretic compression curve that provides a smoother curve than the segmental curve in the HEP model, but does not consider the evolution of particle breakage with mean effective stress. To build upon these previous constitutive models for the isotropic compression curve of sands to high stresses, this study proposes a continuous, nonlinear compression curve model for dry sands under drained conditions and quasi-static loading rates that considers the particle breakage mechanisms behind the transitions in the compression curve with increasing mean effective stress.

Particle Breakage Factors

Several studies have proposed empirical indices or parameters to reflect the amount of particle breakage during shearing (Lade and Yamamuro 1996; Lade et al. 1996; Nakata et al. 1999; Ueng and Chen 2000; Hyodo et al., 2002; Indraratna and Salim 2002; Bazazzadeh et al. 2011; Ghafghazi et al. 2014) or compression (Lee and Farhoomand 1967; Marsal 1967; Murphy 1971; Miura and Yamanouchi 1975; Miura and O'Hara 1979; Hardin 1985; Coop and Lee 1993; Lee and Coop 1995; McDowell et al. 1996; Nakata et al. 2001; Einav 2007a; Einav 2007b; Vilhar et al. 2013). These indices involve the change in individual particle sizes between the particle size distributions before and after loading. Lee and Farhoomand (1967) proposed a breakage indicator expressing the change in a single particle size from their investigation of earth dam filter materials. Miura and O'Hara (1979) introduced a method to compute the changes in particle surface area as an indicator

of particle breakage, which was taken into account new surfaces possibly generated due to particle breakage. The specific surface area of particle size can be estimated by assuming all particles are perfectly spherical.

Marsal (1967) was one of the first studies to define a breakage factor B_M in order to quantify the amount of particle breakage during large scale triaxial tests on rock fill materials. The value of B_M is calculated as the sum of the percent increases in soil retained on each sieve, as follows:

$$B_M = \Sigma(\text{Increase \% retained on all sieves})/100\% \quad (1)$$

A graphical interpretation of the calculation of B_M proposed by Vankov and Sassa (1998) is shown in Figure 2(a) for a dry sand specimen isotropically compressed to 160 MPa under drained conditions. Theoretically, the percent decrease in the amount retained on the larger sieves (shown as small b's in Fig. 2a) should be equal to the percent increase in the amount retained on the smaller sieves (shown as large B's in Fig. 2a). Marsal (1967) showed that B_M increases with confining stress for triaxial compression shear tests performed on different granular soils.

Hardin (1985) further investigated the quantification of particle breakage during compression and shearing, and proposed that sand specimens have identical "breakage potential" when the specimens share the same initial particle size distribution, and suggested that volumetric strain would cease only when particle breakage stopped and a stable gradation was reached. Hardin (1985) defined the relative breakage index B_r as a quantitative indicator of particle breakage, as follows:

$$B_r = \frac{B_t}{B_p} \quad (2)$$

where B_p is the breakage potential defined as the area between original particle size distribution curves of the sand, which is limited in the lower bound by No. 200 sieve (0.074 mm), and B_t is the total breakage potential defined as the area between the original particle size distribution curve

and the final particle size distribution curve. The amount of particle breakage was quantified by using the relative breakage B_r under same conditions, as shown in Figure 2(b). Further work has been performed on the development of breakage factors, but the factor of Hardin (1985) has still been widely used. For example, Einav (2007a,b) used a continuum damage mechanics (fractal) theory based on the critical state framework to modify Hardin's relative breakage index, and hypothesized that the particle size distribution will start from and an initial grading and ultimately reach a final grading due to shearing and compression. Indraratna and Salim (2002) extended the approach of Ueng and Chen (2000) by linking the energy consumption with Marsal's (1973) breakage factor rather than the increase of surface area.

In this study, both the breakage factors of Marsal (1973) and Hardin (1985) were used to quantify the changes in degree of particle breakage from particle size distributions obtained after isotropic compression of sand specimens to different mean effective stresses. Both factors have certain positive and negative aspects. Marsal's breakage factor B_M is based on the increase in percent passing a single sieve so that the estimated value could change if a different set of sieves is used. It may also overemphasize particle breakage in some cases. However, it allows quantification of the changes in particle breakage as the peak percentage difference between the particle size distributions. Hardin (1985) hypothesized that the potential for particle breakage during isotropic or uniaxial compression increases with an increase in particle size since the probability of having a defect in a particle increases for larger particles. Furthermore, the smaller particles which have been crushed, the less potential for additional breakage. The relative breakage index B_r of Hardin (1985) permits quantification of the particle breakage in a more straightforward way by using the ratio between two different quantities, assuming the distribution of fines (less than 0.074 mm) is less important to the compression behavior.

MATERIAL

Mason sand, acquired from a quarry in Longmont, Colorado, was used in this study. The index properties of the sand are summarized in Table 1. Large batches of sand were pre-processed after collection to remove all particles greater than the #10 sieve using dry sieving. Next, representative samples were taken from this larger batch, and repeated particle size distributions on these samples were found to be nearly identical. During initial characterization, the soil properties were determined from three independent tests to obtain accurate measurements. Mason sand is classified as poorly graded sand (SP) according to the Unified Soil Classification System (USCS), which indicates that the material has a narrow range of particle sizes. Most tests in this study were performed at a relative density of 0.75, which corresponds to a void ratio of 0.57. The shear strength properties of this sand under a void ratio of 0.54 were reported by Svoboda and McCartney (2013). Mason sand contains a mixture of approximately 95% silica and 5% feldspar particles. Lee and Seed (1967) noted that particle mineralogy plays an important role in particle breakage during compression and shearing, and noted that sands with greater amounts of feldspar or mica may have greater amount of particle breakage than pure silica sands.

EXPERIMENTAL APPROACH

The experiments were performed in a high pressure isotropic loading apparatus, which has been made suitable to test soil specimens under different drainage conditions. The experimental setup incorporates an isotropic pressure cell used to contain the soil specimen, and a high-pressure syringe pump (model 65HP from Teledyne Isco) used to pressurize the cell fluid and track changes in volume of the soil specimen. Automotive brake fluid was selected as the cell fluid due to its high bulk modulus (2.068 GPa). When provided a target cell pressure, the system controller in the syringe pump will direct a piston into or out of the pump reservoir at a constant rate until the target

pressure is within ±0.3% of the target pressure point. The isotropic pressure cell consists of a hollow stainless steel cylinder sandwiched between two 50.8 mm-thick plates. A 38.1 mm-thick, 71.1 mm-diameter bottom platen used for mounting of the specimen is integrated into the bottom plate. The cell has drainage ports in the bottom platen which, when open, are used to independently control the pore air and pore water pressures and provide free drainage of fluids. Specifically, the pore air pressure in the specimen is applied via a porous sintered stainless ring embedded in the bottom platen of the pressure cell. The pore water pressure in the specimen can be applied via a saturated high-air entry ceramic disk also embedded in the bottom platen of the pressure cell. Dual neoprene membranes, each with a thickness of 0.64 mm, are used to confine the sand specimen. The key features and system calibration are reported in detail by Mun and McCartney (2015), who also showed pictures and detailed schematics of the different components.

A series of isotropic compression tests with mean total stresses ranging from 10 kPa to 160 MPa were performed on Mason sand with different drainage conditions (drained and undrained) for two different degrees of saturation (air dry conditions, $S_r = 0.0$ and saturated conditions, $S_r = 1.0$). Isotropic compression tests were conducted on dry sand under both drained and undrained conditions but on saturated sand only under undrained conditions.

The soil specimens were prepared by tamping the dry sand into a neoprene membrane held in place with a metal mold and attached to the bottom pedestal of the cell. The aluminum tamping rod has a diameter of 40 mm and a mass of 200 g. The dry samples were prepared in 5 lifts of equal height by lightly tamping the rod atop the lift surface until reaching the target thickness. For a known mass of soil in each lift, measurements of the lift thickness from the top of the metal mold were used to confirm the target void ratio. The final specimen dimensions were 76.2 mm in both diameter and height (1:1 ratio). Additional tests were performed on dry sand specimens having

initial relative densities of 0.60 and 0.96 to assess the role of initial conditions on the compression response to high mean effective stresses. It should be noted that the specimen preparation procedure may have an important impact on the soil fabric and its behavior (Sadrekarimi and Olson 2012)

For the tests on dry specimens, a rigid top cap without drainage ports was placed on top of the specimen and the membranes were placed around the cap and sealed with an "O"-ring. This rigid top cap was used in the compression tests so that flexible tubing connections to the top cap would not compress under high cell pressures, ensuring that the compression response of the cell would be relatively stiff compared to the specimen. Instead, the drainage was provided from the ports in the bottom platen of the cell previously described. For the tests on saturated sand specimens, the specimens were prepared using the same approach as the dry specimens but were pre-saturated before placement of the rigid top cap. After placement within the membrane, a temporary top cap with drainage ports was placed on the specimen for saturation. Next, a vacuum of -75 kPa was applied to the top of the specimen for approximately 20 minutes to de-air the specimen. Then de-aired water was permitted to flush upwards through the specimen under a very low flow rate while vacuum was maintained on the top of the specimen. Several pore volumes of water were flushed upward through the specimen. Then the vacuum was shut off and the temporary top cap was carefully removed. The rigid top cap was then placed on top of the saturated sand specimen, and the membrane was carefully pulled up around this cap while avoiding air inclusions.

After the specimens were prepared and the cell was assembled, the high-pressure syringe pump was operated at a constant speed to apply a constant volumetric strain rate of 10%/hr (calculated using the initial dimensions of the sand specimen). The changes in cell pressure during operation of the syringe pump depended on the bulk modulus of the different specimens and the drainage

316 conditions. The same loading rate was used in all the experiments performed in the study. A
317 preliminary test with a slower volumetric strain rate of 2%/hr was found to lead to an identical
318 isotropic compression curve.

319 During compression of the saturated sand specimens under undrained compression, a pore
320 water pressure sensor was not employed to measure the change in pore water pressure due to issues
321 in measuring pressure values accurately over a wide range of stresses. Accordingly, the saturation
322 procedure during tests was not verified using a B-value check. However, the compression curves
323 obtained from repeated experiments to different mean stresses were virtually identical and were at
324 least as stiff as that expected theoretically for water. A gradual process of pressure saturation
325 observed by Mun and McCartney (2016) for unsaturated clays loaded in undrained conditions was
326 not observed for these specimens, indicating that they were likely fully saturated. Although the
327 lack of the pore water pressure sensor does not permit interpretation of the tests in undrained
328 conditions in terms of mean effective stress, these tests are still useful to confirm whether particle
329 breakage occurs during application of high mean total stresses due to potential differences in the
330 compressibility values of the sand skeleton and pore water.

331 Dry sands specimens were tested with both free drainage of air (drained conditions) and
332 without drainage of air (undrained conditions). Although the measurement of the pore air pressure
333 would have been easier than in the case of the pore water pressure measurement in the tests under
334 undrained conditions, this was also not measured. Accordingly, the effects of pore air pressure
335 generation can only be assessed through comparison of the shapes of the compression curves
336 plotted in terms of mean total stress. In the case of drained compression of dry sand, the air was
337 permitted to drain through the drainage port connected to the bottom platen. After isotropic
338 compression of the different dry sand specimens to mean total stresses of 10, 20, 40, 80, and 160

MPa, each specimen was unloaded, the particle size distribution was measured, and breakage factors were calculated using both Marsal's breakage factor B_M and Hardin's relative breakage index B_r to assess the impact of drainage conditions on soil particle breakage under different stress states.

In the tests on dry sand specimens isotropically compressed to mean stresses greater than 80 MPa, cementation was visually observed after removal of the specimen from the cell. Specifically, the dry sand specimens were able to stand up under their own weight as a cohesive unit that had to be broken apart with a mortar and pestle to measure the particle size distribution). Although the tensile strength could have been measured indirectly using a Brazilian test to quantify this cementation, this was not performed in this study. It is possible that the visually-observed cementation was caused by inter-particle bonding formed at the particle contacts, which may have much larger stress magnitudes than the average mean stress applied to the specimen (de Bono et al. 2012). Interlocking associated with angular, broken particles filling the voids may have also occurred. No cementation was observed in the saturated sand specimens compressed in undrained conditions regardless of the mean total stress applied. This further indicates that the effective stress did not change in the undrained tests on saturated specimens.

EXPERIMENTAL RESULTS

Isotropic Compression Response of Dry and Saturated Sand

The isotropic compression curves for dry and saturated Mason sand specimens under different drainage conditions are shown in Figure 3. For each of the drainage conditions investigated, the individual isotropic compression tests on different specimens having the same initial void ratio tended to correspond well with each other up to the mean stresses at which each test was unloaded, confirming the repeatability of the experimental results. Further, for each of the drainage

conditions evaluated, the void ratios of the sand specimens are plotted as a function of mean stress on both logarithmic and natural scales because the use of a logarithmic scale was found to distort the interpretation of the slopes of the compression curves at high mean stresses. The isotropic compression curves of dry sand in drained conditions in Figure 3(a) seem to indicate a conventional bilinear response for the loading curves, although a slight hardening response similar to that observed in section C-D in Figure 1 is observed at mean effective stresses greater than 30 MPa. The unloading curves are log-linear except in the cases of unloading from mean effective stresses of 80 and 160 MPa. Although the slopes of these unloading lines appear to show a softer response (i.e., a greater decrease in void ratio for an increase in mean effective stress), this is distorted by the logarithmic scale. The same isotropic compression curves plotted on a natural scale in Figure 3(b) indicate that the specimens are gradually hardening with increasing mean effective stress, reflecting an asymptotic trend toward a certain void ratio.

The slope of the isotropic compression curve for the dry sand specimen loaded in drained conditions to 160 MPa is shown in Figure 4. The slope of the loading curve starts to decrease at approximately 30 MPa, which can be hypothesized to correspond to the initiation of the transition to void closure. Further, during unloading from a mean effective stress of 160 MPa, the unloading slope is smaller and increases with decreasing mean effective stress but approaches the same slope as the curve for loading from lower mean effective stresses. This means that even though the corresponding unloading branch of the isotropic compression curve for the specimen loaded to 160 MPa in Figure 3(a) appears to be softer, this is not the case and is an artifact of the logarithmic scale. Similar nonlinear compression curves are observed for sand specimens unloaded from mean stresses ranging from 50 to 850 MPa were noted by Miura and Yamanouchi (1975) and Yamamuro et al. (1996b). The isotropic compression curves for dry sand compressed in undrained conditions

(no drainage of pore air) shown in Figure 3(c) and 3(d) are very similar to those for the dry sand under drained conditions, indicating that constraint of the pore air does not have a significant effect on the compression response of dry sand.

The isotropic compression curves of saturated sand specimens in undrained conditions shown in Figure 3(e) are stiffer than those tested under drained conditions, and the slope of the entire compression response from 10 kPa to 160 MPa is nearly linear when plotted on a natural scale in Figure 3(f). Although the effective stress was not expected to change in this test due to the low compressibility of water, differences between the compressibility of the water and soil skeleton may lead to some relative movement between the phases during isotropic compression. The compressibility of water may depend on the applied pressure, following a quadratic or cubic relationship for pressures greater than 10 MPa (Hayward 1967). Although this nonlinearity is small enough that the bulk modulus of water can be approximated by a constant secant modulus, the pressure dependent bulk modulus of water at a temperature of 20 °C was assumed to follow the cubic relationship of Finnemore and Franzini (2002) shown in Figure 5(a). The volume change of the saturated sand specimen isotropically compressed in undrained conditions to 160 MPa is compared with that of water having a nonlinear bulk modulus in Figure 5(b). The saturated sand specimen compressed in undrained conditions shows a stiffer response than that of water, with a difference of approximately 19% at 160 MPa that of water may be due to the greater stiffness of the individual sand particles.

To further consider the impact of drainage conditions on the compression responses of dry and saturated Mason sand, comparisons of the isotropic compression curves for different testing conditions over the same stress range (160 MPa) are shown in Figures 6(a) and 6(b). The drained compression curves are shown in terms of mean effective stress (equal to the mean total stress)

while the undrained compression curves are shown in terms of the mean total stress as it was not possible to calculate the mean effective stress in the undrained compression tests. For the dry sand specimens, the isotropic compression curve for undrained conditions shows a slightly stiffer response than curve for drained conditions, but the difference is not significant. The results indicate that the isotropic compression curve for dry sand under drained conditions has a slightly greater slope in the region between 30 and 100 MPa (0.33) than that of dry sand under undrained conditions in the same region (0.29). This may be due to the finite compressibility of air, which although large, may lead to changes in the stress state that changes the constraint on particle rearrangement. The isotropic compression curve for saturated sand under undrained conditions indicates a much stiffer and more linear response than the curves for dry sand.

Particle Breakage during Isotropic Compression

Particle size distributions for the Mason sand specimens were determined before and after testing, and are shown in Figures 7(a), 7(b), and 7(c) for the different drainage conditions. A general observation that can be made from evaluating these curves is that the percent retained on all of the sieves with opening sizes smaller than 0.83 mm increased, but the amount retained on the sieve with an opening size of 0.83 mm did not change. Because Mason sand is a mixture of quartz and feldspar particles, it is possible that the larger particles are stronger (i.e., are quartz) and the smaller particles are softer (i.e., are feldspar). Tsoungui et al. (1999) investigated the cushioning effect in the fragmentation process, suggesting that the larger particles could be cushioned by surrounding smaller particles while neighboring smaller particles continue to crush. The changes in the key parameters of the particle size distributions are summarized in Table 2. In the case of the isotropic compression tests on dry sand, increases in D_{10}, D_{30}, and D_{60} were observed for each of the mean stress intervals, with slightly lower breakage occurring in the case

of undrained conditions. In the case of isotropic compression of saturated sand in undrained conditions, the changes in D_{10}, D_{30}, and D_{60} were smaller, although the value of D_{10} increased by 25% when reaching a mean total stress of 80 MPa with little further change with beyond this point. Despite this increase in D_{10}, examination of the particle size distributions in Figure 7 indicates that the amount of the fines (particles smaller than 0.075 mm) generated during isotropic compression to 160 MPa was negligible for saturated sand under undrained conditions (a 0.15% increase) but was greater for the dry sands under drained and undrained conditions (7.0 and 7.4% increases, respectively). The small change in the amount of fines for the saturated sand under undrained conditions is attributed to variability between the specimens.

A comparison of the isotropic compression curves of dry sand specimens with different initial relative densities under drained conditions is shown in Figure 8(a). Consistent with the observations of previous studies (e.g., Hendron 1963; Lee and Seed 1967; Golightly 1990; Vilhar et al. 2013), the isotropic drained compression curves of specimens with different initial relative densities converge to a unique compression curve at mean effective stresses of approximately 20 MPa. Comparisons of the particle size distributions for specimens having different initial relative densities after application of a mean effective stress of 160 MPa are shown in Figure 8(b). The particle size distributions are nearly identical regardless of the initial relative densities, which is also confirmed from the particle size characteristics for these specimens shown in Table 3. Although it is expected from the literature that denser samples undergo less breakage than looser ones to reach a given stress on the normal compression line (Roberts and de Souza 1958; DeBeer 1963; Hendron 1963; Coop and Lee 1993; Hagerty et al. 1993; Lade et al. 1996; Nakata et al. 2001a, 2001b; Mesri and Vardhanabhuti, 2009) the experimental results suggest the impact of the initial void ratio has no effect on particle breakage after application of a mean effective stress

160 MPa. Similar behavior was noted by several researchers who observed that the initial void ratio has the greatest effect at low mean effective stresses, but becomes irrelevant after uniaxial compression beyond mean stresses of 30 MPa (Hendron 1963; Yamamuro et al. 1996b; Altuhafi and Coop 2011). This observation is similar to the concept of "breakdown stress" proposed by Vesić and Clough (1968), which is defined as the mean stress required to remove all effects of the initial void ratio. Although difficulties are encountered with the breakdown stress concept when considering particle breakage, it plays a role when using the state parameter concept (Been and Jefferies 1985).

The evolution in the particle breakage factor B_M of Marsal (1967) and the particle breakage index B_r of Hardin (1985) during isotropic compression for different testing conditions are shown in Figure 9, with the numerical values summarized in Table 4. The breakage factors shown in Figure 9(a) for dry sand were observed to increase nonlinearly with mean stress following a power law relationship. This type of relationship was also observed for trends in B_r measured for uniaxial compression tests on silty sand in drained conditions by Vilhar et al. (2013). The values of the particle breakage factors were similar for the dry sand under drained and undrained conditions. The slightly smaller values observed for the dry sand under undrained conditions may be due to the interpretation of these data points in terms of total stress. For dry sand under drained conditions, the percent increases in Marsal's B_M and Hardin's B_r after reaching a mean stress of 160 MPa were 5.8% and 2.6%, respectively. The increases in the breakage factors with mean stress could be approximated using the power law relationships shown in Figure 9(a), with the parameters of the power law relationships for the dry sand under different testing conditions summarized in Table 5. The evolution in the breakage factors with mean total stress for the saturated sand specimens isotropically compressed in undrained conditions shown in Figure 9(b) show B_r is approximately

zero for all the mean total stresses indicating negligible particle breakage, while B_M is also small but shows an increasing trend with mean total stress. A disadvantage of Marsal's breakage factor is that it has no upper limit and can thus overemphasize the amount of particle breakage in some cases and can be affected by small differences in the smallest particle size in Figure 7(c). The changes in B_M and B_r for dry sand specimens with different initial relative densities isotropically compressed are presented in Figure 9(c). Although B_M is slightly greater than B_r for specimens with greater initial relative densities as shown in Table 4, the values of B_M and B_r do not change significantly with the initial relative density after compression to mean effective stresses of 160 MPa. Accordingly, it can be assumed that the initial relative density does not have an impact on particle breakage of Mason sand at high mean effective stresses in this range.

HIGH STRESS COMPRESSION CURVE MODEL FOR SAND BASED ON PARTICLE BREAKAGE

The results of the isotropic compression tests on dry sand and the corresponding breakage factors can be used to define a nonlinear model to represent the compression response of dry sands to high mean effective stresses. Because the value of Hardin's relative breakage index was scaled between 0 and 1, it was used in the development of this model instead of Marsal's breakage factor. The following exponential relationship was developed to represent the shape of the isotropic drained compression curve of dry sand during loading from an initial void ratio e_0:

$$e = e_0 \times \mathrm{e}^{-\alpha \cdot (100 \times B_r)^{\delta}} - \beta \cdot p' \qquad (3)$$

where p′ is the mean effective stress, e_0 is the initial void ratio, and α, β, and δ are empirical coefficients. The value of B_r is assumed to be stress-dependent up to p′ of 160 MPa during isotropic compression following the power-law relationship shown in Figure 9(a) with the parameters given in Table 5. It also assumes that the mean effective stress is in quasi-static conditions. Further, this

relationship is assumed to be valid for dry Mason sand specimens with different initial void ratios, and that the evolution in B_r with mean effective stress measured for the specimens with $e_0 = 0.57$ can be applied to the specimens with different initial void ratios as their B_r values after reaching a mean effective stress of 160 MPa shown in Figure 9(c) are similar.

Modeling the unloading curves for dry sand is more complex since linear elastic behavior is noted after when unloading from mean effective stresses below 40 MPa, while nonlinear elasto-plastic behavior is noted during unloading from higher mean effective stresses. Further, the results in Figures 3(a) and 3(c) indicate that the amount of nonlinearity increases when the Mason sand specimens are unloaded from higher mean effective stresses, potentially due to the cementation caused by inter-particle bonding and greater interlocking associated with broken particles filling the voids. For the effect of breakage behavior on saturated sand for mean effective stresses less than 20 MPa, the conventional log-linear unloading curve can be used:

$$e = -\kappa \ln \frac{p}{p^{max}} \tag{4}$$

where p^{max} is the maximum mean effective stress applied during loading. For unloading from mean effective stresses greater than 30 MPa, the two following relationships can be used to fit the unloading curve:

$$\begin{aligned} p' > \frac{p^{max}}{100 \times B_r^{max}}: \quad & e = \gamma \cdot e^{max} \times \mathrm{e}^{-\chi \cdot p^{\wedge}} - \eta \cdot p' \\ p' < \frac{p^{max}}{100 \times B_r^{max}}: \quad & e = -\kappa \ln \frac{p'}{p^{max}} \end{aligned} \tag{5}$$

where e^{max} is the void ratio at the maximum applied mean stress p^{max}, B_r^{max} is Hardin's relative breakage index after loading to p^{max}, and γ, χ, and η are empirical fitting parameters. The use of

two curves captures the trend in nonlinearity in the curves by incorporating the evolution of the breakage factor in the formulation, but also reflects the fact that the unloading curves all have the same slope at lower mean effective stresses. Other models such as the non-linear elastic formulation of Pestana and Whittle (1995) with an incremental bulk modulus could be used to fit the observed trends in the data.

The models for the loading and unloading curves were formulated to match the experimental isotropic drained compression curves for dry Mason sand up to 160 MPa under different drainage conditions, and the model parameters for the different cases considered are summarized in Table 6. The isotropic compression curves of the dry sand specimens in drained conditions loaded to different mean stresses is shown in Figure 10(a) along with the model prediction curves. The formulated model is able to capture the shape of the compression curves at both low and high mean effective stresses, and also reflects the transition in the shape of the unloading curves for specimens loaded to mean stresses greater than 30 MPa. The void ratio from the model prediction was compared with the measured data and the percentage of void ratio difference was estimated to quantify the accuracy of the model prediction. It was found that the maximum difference between the measured and predicted void ratios is less than 5%. Although the model was only plotted up to 160 MPa, the form of the model is such that it can provide a consistent shape to that shown in the hypothetical uniaxial compression curve in Figure 1, as well as the hysteretic nonlinear model of Akers (2001) up to the point of void closure.

The drained compression curves of sand specimens with different initial relative densities are shown in Figure 10(b) along with the model prediction curves. Again, a good match with a void ratio difference of less than 3% was observed between test results and the model prediction, which indicates that the trends in the breakage factor for dry sand can be applied to sands compressed in

drained conditions to mean stresses of up to 160 MPa under a constant, quasi-static, volumetric strain rate of 10%/hr. The fact that the difference of the breakage factors (B_M, B_r) at 160 MPa for the sands with different initial densities are less than 5-6% confirms that the evolution of particle breakage with mean effective stress can be assumed to be independent of the initial relative density. The effect of initial relative density on the isotropic compression behavior of the sand is dominated by the values of the empirical parameters α and β in the formulated model. Based on the proposed model, a similar relationship could be formulated using the Marsal's breakage factor B_M, but Hardin's relative breakage index B_r was used because it is normalized between 0 and 1 and provides a more predictable range of values.

CONCLUSIONS

The results from a series of isotropic compression tests on dry and saturated sand under different pore fluid drainage conditions up to a mean stress of 160 MPa indicate that the isotropic compression response of granular materials is influenced by the trends in particle breakage, and that pore fluid drainage conditions can influence both the shape of the compression curve and the quantity of particle breakage. An empirical compression curve model for the drained, quasi-static isotropic compression response of dry sand was proposed that incorporates the evolution in Hardin's relative breakage index B_r with mean effective stress was developed that showed a good match to the experimental data. The following specific conclusions can be drawn from this study:

- The isotropic compression curve for dry sand having an initial void ratio of 0.57 under drained conditions follows a nonlinear trend with increasing mean effective stress that reflects the transition to void ratio at high mean effective stresses, reaching a void ratio of 0.036 at a mean effective stress of 160 MPa.

- The unloading response of dry sand was observed to be nonlinear for mean effective stresses greater than 30 MPa potentially due to the cementation caused by inter-particle bonding and greater interlocking associated with broken particles filling the voids.
- The compression curves of dry sand under drained and undrained conditions were found to be similar, with the undrained tests showing a slightly stiffer response. Similar trends in particle breakage were observed for both drainage conditions, indicating that the high compressibility of air causes it not to provide a major constraint on particle rearrangement.
- The particle size distributions measured after isotropic compression of dry sand in drained conditions up to a mean stress of 160 MPa under a constant, quasi-static, volumetric strain rate of 10%/hr indicated an increase in the amount of fines generated by approximately 7%. The amount of particle breakage was quantified using different breakage factors that were found to follow a power law relationship with mean stress.
- Isotropic compression tests on saturated sand in undrained conditions showed a linear compression curve that was stiffer than water. Negligible particle breakage and no cementation were observed in these tests after unloading, likely because there was a negligible change in mean effective stress in the undrained tests.
- Specimens with different initial relative densities from 0.51 to 0.61 showed similar amount of particle breakage behavior after application of a mean effective stress of 160 MPa under drained conditions, and the compression curves were found to be identical after a mean effective stress of 20 MPa.
- The empirical model for the isotropic compression curve of dry sand under drained conditions was found to match the experimental data well with a maximum difference between the predicted and measured void ratios of 5%. The model was successfully capture the nonlinearity

584 in the compression curves at both high and low mean effective stresses, and is more physically
585 based than previous nonlinear compression curves as it incorporates Hardin's relative breakage
586 index as a parameter.

587 **ACKNOWLEDGEMENTS**

588 Funding for this research was provided by Office of Naval Research (ONR) grant N00014-11-
589 1-0691. The opinions in this paper are those of the authors alone.

590 **REFERENCES**

591 Akers, S.A. (2001). Two-Dimensional Finite Element Analysis of Porous Geomaterials at
592 Multikilobar Stress Levels. Ph.D. Thesis. Virginia Tech, VA.
593 Akers, S.A., Reed, P.A., and Ehrgott, J.Q. (1986). WES High-pressure Uniaxial Strain and Triaxial
594 Shear Test Equipment. Miscellaneous Paper SL-86-11. Vicksburg, MS.
595 Akers, S.A., Adley, M.D., and Cargile, J.D. (1995). Comparison of constitutive models for
596 geologic materials used in penetration and ground shock calculations. Proc. 7th International
597 Symposium on Interaction of the Effects of Munitions with Structures, Mannheim, Germany.
598 Altuhafi, F. N., and Coop, M. R. (2011). "Changes to particle characteristics associated with the
599 compression of sands." Géotechnique. 61(6), 459-471. 10.1680/geot.9.P.114
600 Bandini, V., Coop, M.R. (2011). "The influence of particle breakage on the location of the critical
601 state line." Soils and Foundation. 51(4), 591-600.
602 Bazazzadeh H, Kalantary F, Asakereh A. (2011). "An investigation on the effect of particle
603 breakage on rockfill constitutive parameters." Electronic Journal of Geotechnical Engineering.
604 15, 847-864.

Becker, E., Chan, C.K., and Seed, H.B. (1972). "Strength and deformation characteristics of rockfill materials in plain strain and triaxial compression tests." Report TE-72-3, Office of Research Services, University of California Berkeley, CA.

Been, K., and Jefferies, M.G. (1985). "A state parameter for sands." Géotechnique 35, 99–112.

Been, K., Jefferies, M.G., and Hachey, J. (1991). "The critical state of sands." Géotechnique. 41(3), 365-381.

Bishop, A.W., Webb, D.L., and Skinner, A.E. (1965). "Triaxial tests on soil at elevated cell pressures." Proc. 6th International Conference on Soil Mechanics and Foundation Engineering, University of Toronto Press, Toronto, Canada, Vol. 1, 170-174.

Bishop, A.W. (1966). "The strength of soils as engineering materials." Géotechnique. 16(2), 91-130.

Biarez, J. and Hither, P. (1994). Elementary Mechanics of Soil Behaviour. A.A. Balema, Rotterdam.

Charlie, W.A., Ross, C.A., Pierce, S.J. (1990). "Split-Hopkinson pressure bar testing of unsaturated sand." Geotechnical Testing Journal. 13(4), 291–300.

Colliat-Dangus, J.L., Desrues, J., and Foray, P. (1988). "Triaxial testing of granular soil under elevated cell pressure." Advanced Triaxial Testing of Soil and Rock, ASTM STP 977, 290-310.

Coop, M.R., and Lee, I.K. (1993). "The behaviour of granular soils at elevated stresses." Predictive Soil Mechanics. Thomas Telford, London. 186-198.

DeBeer, E.E. (1963). "The scale effect in the transposition of the results of deep sounding tests on the ultimate bearing capacity of piles and caisson foundations." Géotechnique, 13(1), 39-75.

627 de Bono, J., McDowell, G. R., and Wanatowski, D. (2012) "Discrete element modelling of a
628 flexible membrane for triaxial testing of granular material at high pressures." Géotechnique
629 Letters, 2(4), 199-203, 10.1680/geolett.12.00040.
630 Einav, I. (2007a). "Breakage Mechanics-Part I: Theory," Journal of the Mechanics and Physics of
631 Solids, 55(6), 1274-1297. 10.1016/j.jmps.2006.11.003
632 Einav, I. (2007b). "Breakage Mechanics-Part II: Modelling granular materials, 55(6), 1298-1320.
633 10.1016/j.jmps.2006.11.004
634 Ezaoui, A., Lecompte, T., Di Benedetto, H., and Garcia, E. (2011). "Effects of various loading
635 stress paths on the stress–strain properties and on crushability of an industrial soft granular
636 material." Granular Matter 13(4), 283-301.
637 Farr, J. V., and Woods, R. D. (1988). "Device for evaluating one-dimensional compressive loading
638 rate effects." Geotechnical Testing Journal, 11(4), 269-275.
639 Field, J.E., Walley, S.M., Proud, H.T., Goldrein, H.T., Siviour, C.R. (2004). "Review of
640 experimental techniques for high rate deformation and shock studies." International Journal of
641 Impact Engineering. 30(7), 725-75.
642 Finnemore, E.J, and Franzini J.B. (2002). Fluid mechanics with engineering applications. 10th ed.
643 WCB/McGraw-Hill, U.S.A.
644 Fukuoka, H., Sassa, K., Shima, M. (1990). "Shear characteristics of sandy soils and clayey soils
645 subjected to the high-speed and high-stress ring shear tests." Annuals of Disaster Prevention
646 Research Institute of Kyoto University B-1 (33), 179–190 (in Japanese).
647 Fukumoto, T. (1992). "Particle breakage characteristics in granular soils." Soils and Foundations.
648 32(1), 26-40.

649 Ghafghazi, M., Shuttle, D.A., DeJong, J.T. (2014). “Particle breakage and the critical state of sand.”
650 Soils and Foundations. 54(3), 451-461.
651 Golightly, C.R. (1990). Engineering Properties of Carbonate Sands. Ph.D. Dissertation, Bradford
652 University.
653 Gupta A.K. (2000). Constitutive Modelling of Rockfill Material. PhD Thesis. Delhi, India: Indian
654 Institute of Technology.
655 Hagerty, M.M., Hite, D.R., Ullrich, C.R., and Hagerty, D.J. (1993). “One-dimensional high-
656 pressure compression of granular media.” Journal of Geotechnical Engineering. 119(1), 1-18.
657 Hall, E.B., and Gordon, B.B. (1963). “Triaxial testing with large-scale high pressure equipment.”
658 *In* Laboratory shear testing of soils. ASTM STP 361, 315-328.
659 Hardin, B.O. (1985). “Crushing of soil particles.” Journal of Geotechnical Engineering. 111(10),
660 1177-1192.
661 Hayward A.T.J. (1967). “Compressibility equations for liquids: a comparative study.” British
662 Journal of Applied Physics. 18, 965-977.
663 Hendron, A. (1963). The Behavior of Sand in One-Dimensional Compression. PhD Dissertation,
664 University of Illinois, Urbana-Champaign.
665 Hendron, A.J., Davisson, M.T. and Parola, J.F. (1969). Effect of Degree of Saturation on
666 Compressibility of Soils from the Defense Research Establishment Suffield. US Army
667 Engineer Waterways Experiment Station, Vicksburg, Ms.
668 Hirschfield, R.C., and Poulos, S.J. (1963). “High pressure triaxial tests on a compacted sand and
669 an undisturbed silt.” Laboratory Shear Testing of Soils. ASTM STP 361, 329-339.

Holland, C.N. (1971). An Investigation of the Strength-Deformation Characteristics of Two Soils Tested under High Confining Pressures in the Triaxial Cell." PhD Dissertation, Georgia Institute of Technology.

Hyodo, M., Hyde, A. F. L., Aramaki, N., and Nakata, Y. (2002). "Undrained montonic and cyclic shear behaviour of sand under low and high confining stresses." Soils and Foundations. 42(3), 63-76.

Indraratna, B., and Salim, W. (2002). "Modeling of particle breakage in coarse aggregates incorporating strength and dilatancy." Geotechnical Engineering. 155(4), 243-252.

Kabir, M.E., Song, B., Martin, B.E., and Chen, W. (2010). Compressive Behavior of Fine Sand. Sandia Report SAND2010-2289, 72.

Konrad J.M. (1998). "Sand state from cone penetrometer tests: a framework considering grain crushing stress." Géotechnique. 48(2), 201-215.

Luo, H., Du, Y., Hu, Z., Cooper, W.L., and Lu, H. (2015), "High-strain rate compressive behavior of glass beads under confinement." Experimental Mechanics. 55(5), 935-950.

Lade, P.V., Yamamuro, J.A., and Bopp, P.A. (1996). "Significance of particle crushing in granular materials." Journal of Geotechnical Engineering. 122(4), 309-316.

Lade, P.V. and Yamamuro, J.A. (1996). "Undrained sand behavior in axisymmetric tests at high pressure." Journal of Geotechnical Engineering. 122(2), 120-129.

Lee, I.K. and Coop, M.R. (1995). "The intrinsic behaviour of a decomposed granite soil." Géotechnique. 45(3), 545-561.

Lee, K.L. and Farhoomand, I. (1967). "Compressibility and crushing of granular soils in anisotropic triaxial compression." Canadian Geotechnical Journal. 4(1), 68-86.

692 Lee, K.L. and Seed, H.B. (1967). “Drained strength characteristics of sands.” Journal Soil
693 Mechanics and Foundation Div. 93(6), 117-141.
694 Leslie D. D. (1975). “Shear strength of rockfill.” South Pacific Division Corps of Engineering
695 Laboratory, California, Physical Properties of Engineering Study No. 526.
696 Lo, K.Y. and Roy, M. (1973). “Response of particulate materials at high pressures.” Soils and
697 Foundations. 13(1), 1-14.
698 Marachi, N.D., Chan, C.K., Seed, H.B., and Duncan, J.M. (1969). Strength and Deformation
699 Characteristics of Rockfill Materials. Rep. No. TE-69-5, University of California, Berkeley.
700 Marsal, R.J. (1967). “Large scale testing of rockfill materials.” Journal of the Soil Mechanics and
701 Foundations Division. 93(SM2), 27-43.
702 Martin, B.E., Chen, W., Song, B, and Akers, S.A. (2009). “Moisture effects on the high strain-rate
703 behavior of sand.” Mechanics of Materials. 41(6), 786-798.
704 Mazanti, B.B., and Holland, C.N. (1970). “Study of soil behavior under high pressure.” Contract
705 Report S-70-2.
706 Mesri, G., and Vardhanabhuti, B. (2009). “Compression of granular materials.” Canadian
707 Geotechnical Journal 46, 369-392. 10.1139/T08-123
708 McDowell, G.R., Bolton, M.D., and Robertson, D., (1996). “The fractal crushing of granular
709 materials.” Journal of the Mechanics and Physics of Solids. 44 (12), 2079-2102.
710 McDowell, G.R. and Bolton, M.D. (1998). “On the micro mechanics of crushable aggregates.”
711 Géotechnique. 48(5), 667–679.
712 McDowell, G. R. (2002). “On the yielding and plastic compression of sand.” Soils and Foundations.
713 42(1), 139-145.

714 Miura, N. and Yamanouchi, T. (1975). “Effect of water on the behavior of a quartz-rich sand under
715 high stresses.” Soils and Foundations. 15(4), 23-34.
716 Miura, N. and O’Hara, S. (1979). “Particle crushing of decomposed granite soil under shear
717 stresses.” Soils and Foundations. 19(3), 1-14
718 Moral, R.J., Danielson, K.T., and Ehrgott, J.Q., Jr. (2010). Tactical Wheeled Vehicle Survivability:
719 Comparison of Explosive-soil-air-structure Simulations to Experiments using the Impulse
720 Measurement Device. Technical Report ERDC/GSL TR-10-27, Vicksburg, MS.
721 Muir Wood, D. (2008). “Critical states and soil modeling.” Deformational Characteristics of
722 Geomaterials. 1, IOS Amsterdam, 51-72.
723 Muir Wood, D., and Maeda, K. (2008). “Changing grading of soil: effect on critical states.” Acta
724 Geotechnica. 3(3), 3-14.
725 Mun, W. and McCartney, J.S. (2015). “Compression mechanisms of unsaturated clay under high
726 stress levels.” Canadian Geotechnical Journal. 52(12), 1-14. 10.1139/cgj-2014-0438.
727 Mun, W. and McCartney, J.S. (2016). “Constitutive model for the undrained compression of
728 unsaturated Clay.” ASCE Journal of Geotechnical and Geoenvironmental Engineering. 1-10.
729 10.1061/(ASCE)GT.1943-5606.0001635. 04016117.
730 Murphy, D.J. (1971). “High pressure experiments on soil and rock.” Proc. 13th Symposium on
731 Rock Mechanics. 691-714.
732 Nakata, Y., Hyde, A.F.L., Hyodo, M., and Murata, H., (1999). “A probabilistic approach to sand
733 particle crushing in the triaxial test.” Géotechnique. 49(5), 567-583.
734 Nakata, Y., Kato, Y., Hyodo, M., Hyde, A.F.L., and Murata, M. (2001a). “One-dimensional
735 compression behavior of uniformly graded sand related to single particle crushing strength.”
736 Soils and Foundations. 41(2), 39-51.

737 Nakata, Y., Hyodo, M., Hyde, A.F., Kato, Y., and Murata, H. (2001b). "Microscopic particle
738 crushing of sand subjected to high pressure one-dimensional compression." Soils and
739 Foundations. 41(1), 69-82.
740 Novello, E.A. and Johnston, I.W. (1989). "Normally consolidated behaviour of geotechnical
741 materials." In: Proceedings of the 12th International Conference on Soil Mechanics, Rio de
742 Janeiro, 3. 2095-2100.
743 Omidvar, M., Iskander, M., and Bless, S. (2012) "Stress-strain behavior of sand at high strain rates."
744 International Journal of Impact Engineering. 49(November), 192-213
745 Oldecop, L. A. and Alonso, E. E. (2003). "Suction effects on rockfill compressibility."
746 Géotechnique. 53(2), 289-292. 10.1680/geot.2003.53.2.289.
747 Pestana, J.M., and Whittle, A.J. (1995). "A compression model for cohesionless soils."
748 Géotechnique. 45(4), 611-631.
749 Roberts, J.E., and de Souza, J.M. (1958). "The compressibility of sands." Proceedings of the
750 American Society for Testing and Materials, 58. 1269-1272.
751 Richart, F.E., Jr., Hall, J.R. and Woods, R.D. (1970). Vibrations of Soils and Foundations,
752 Prentice-Hall, Inc, Englewood Cliffs, NJ.
753 Russell, A.R. and Khalili, N. (2002). "Drained cavity expansion in sands exhibiting particle
754 crushing." International Journal for Numerical and Analytical Methods in Geomechanics.
755 26(4), 323-340.
756 Sadrekarimi, A. and Olson, S.M. (2012). "Effect of sample preparation method on critical state
757 behavior of sands." Geotechnical Testing Journal, ASTM, 35(4), 548-562.
758 Salim W., and Indraratna B. (2004) "A new elasto-plastic constitutive model for coarse granular
759 aggregates incorporating particle breakage." Canadian Geotechnical Journal. 41(4), 657-671.

760 Schmertmann, J. H. (1991). “The mechanical aging of soils.” Journal of the Geotechnical
761 Engineering Division, ASCE. 117(9), 1288-1330.
762 Sowers, G. F., Williams, R. C. & Wallace, T. S. (1965). “Compressibility of broken rock and
763 settlement of rockfills.” Proc. 6th International Conference of Soil Mechanics, Montreal 2,
764 561-565.
765 Svoboda, J. and McCartney, J.S. (2013). “Shearing rate effects on dense sand and compacted clay.”
766 Chapter 47 in Dynamic Behavior of Materials, Vol. 1. B. Song, ed. Springer, Vienna. 389-395.
767 Tai, T. (1970). Strength and Deformation Characteristics of Cohesionless Materials at High
768 Pressures. Ph.D. Dissertation. Duke University.
769 Tsoungui, O., Vallet, D., Charmet, J.C. (1999). “Numerical model of crushing of grains inside
770 two-dimensional granular materials.” Powder Technology. 105(1-3), 190-198.
771 Ueng, T.S., Chen, T.J. (2000). “Energy aspects of particle breakage in drained shear of sands.”
772 Géotechnique. 50(1), 65-72.
773 Wang, J., and Yan, H. (2013). “On the role of particle breakage in the shear failure behavior of
774 granular soils by DEM.” International Journal for Numerical and Analytical Methods in
775 Geomechanics. 37(8), 832-854.
776 Whitman, R.V., Miller, E.T., and Moore, P.J. (1964). “Yielding and locking of confined sand.”
777 Journal of the Soil Mechanics and Foundations Division, ASCE, 90(4), 57-84
778 Whitman, R.V. (1970). The Response of Soils to Dynamic Loading. Report No. 26, Final Report.
779 Vicksburg, Mississippi: U.S. Army Engineer Waterways Experiment Station.
780 Wu S., Gray D.H. and Richart F.E. Jr. (1984). “Capillary effects on dynamic modulus of sands
781 and silts.” Journal of Geotechnical Engineering, ASCE, 110(9), 1188-1203.

782 Vankov, D.A., and Sassa, K. (1998). “Energy approach to evaluation of grain crushing.” Proc.
783 IUFRO Division 8 Conference on Environmental Forest Science, 19-23 Oct., Kyoto. Springer-
784 Science and Business Media. Dordrecht, Netherlands. 615-622.
785 Verdugo, R. and Ishihara, K. (1996). “The steady state of sandy soils.” Soils and Foundations.
786 36(2), 81-91.
787 Vesić, A.S., and Clough, G.W. (1968). “Behaviour of granular materials under high stresses.”
788 Journal of the Soil Mechanics and Foundations Division. 94(SM3), 661-688.
789 Veyera, G. (1994). Uniaxial Stress-Strain Behavior of Unsaturated Soils at High Strain Rates. Final
790 Report Wright Laboratory Flight Dynamics Directorate. WL-TR-93-3523.
791 Vilhar, G., Jovicic, V., and Coop, M.R. (2013). “The role of particle breakage in the mechanics of
792 a non-plastic silty sand.” Soils and Foundations. 53(1), 91-104.
793 Yamamuro, J.A., Lade, P.V. (1993). “Effects of strain rate on instability of granular soils.”
794 Geotechnical Testing Journal. 16(3), 304–313.
795 Yamamuro, J.A., and Lade, P.V. (1996a). “Drained sand behavior in axisymmetric tests at high
796 pressures.” Journal of Geotechnical Engineering. 122(2), 109-119.
797 Yamamuro, J.A., Bopp, P. A., and Lade, P. V. (1996b). "One-dimensional compression of sands
798 at high pressures." Journal of Geotechnical Engineering 122(2), 147-154.
799 Zhang, Y.D. and Buscarnera, G. (2014). “Grainsize dependence of clastic yielding in unsaturated
800 granular soils.” Granular Matter 16(4), 469-483. 10.1007/s10035-014-0491-7
801 Zimmerman, H.D., Shimano, R.T., and Ito, Y.M. (1992). Early-Time Ground Shock from Buried
802 Conventional Explosives: User's Guide for SABER-PC/CWE. Instruction Report SL-92-1.
803 Vicksburg, MS: U.S. Army Engineer Waterways Experiment Station.
804

LIST OF TABLE AND FIGURE CAPTIONS

FIG. 9: Comparison of the changes in Marsal's breakage factor (B_M) and Hardin's relative breakage index (B_r) of Mason sand during isotropic compression to different mean stresses with different testing conditions: (a) Drained/Undrained (Dry); (b) Undrained (Saturated); (c) Drained with different initial relative densities (Dry) to 160 MPa

FIG. 10: Comparison of the simulated (dashed black lines) and experimental (dotted points) isotropic drained compression curves for dry sands: (a) Loading and unloading curves for dry sand with an initial relative density of 0.75; (b) Loading curves for dry sand with different initial relative densities

Table 1: Index properties of Mason sand

Property	Value	Units
Particle size at 10% passing, D_{10}	0.15	mm
Particle size at 30% passing, D_{30}	0.28	mm
Particle size at 50% passing, D_{50}	0.50	mm
Coefficient of uniformity, C_u	3.33	-
Coefficient of curvature, C_c	1.05	
Specific gravity, G_s	2.62	-
Minimum void ratio, e_{min}	0.50	-
Maximum dry density, ρ_{max}	1.74	kg/m^3
Maximum void ratio, e_{max}	0.78	-
Minimum dry density, ρ_{min}	1.47	kg/m^3

Table 2: Summary of changes in the particle size distribution of Mason sand during isotropic compression to different mean stresses p′ (drained) or p (undrained)

Property	Drainage and specimen conditions	Before testing	After compression to different mean stresses p′ (drained) or p (undrained)				
			10 MPa	20 MPa	40 MPa	80 MPa	160 MPa
D_{10} (mm)	Drained (Dry)	0.15	0.12	0.12	0.09	<0.075	<0.075
	Undrained (Dry)		0.12	0.12	0.09		
	Undrained (Sat.)		0.15	0.15	0.15	0.12	0.12
D_{30} (mm)	Drained (Dry)	0.28	0.27	0.27	0.21	0.19	0.14
	Undrained (Dry)		0.27	0.27	0.22	0.19	0.13
	Undrained (Sat.)		0.28	0.28	0.28	0.28	0.28
D_{60} (mm)	Drained (Dry)	0.50	0.50	0.50	0.48	0.45	0.41
	Undrained (Dry)		0.50	0.50	0.48	0.45	0.40
	Undrained (Sat.)		0.50	0.50	0.50	0.50	0.50
C_u	Drained (Dry)	3.33	4.17	4.17	5.33	<6.00	<6.00
	Undrained (Dry)		4.17	4.17	5.33	<6.00	<6.00
	Undrained (Sat.)		3.33	3.33	3.33	4.17	4.17
C_c	Drained (Dry)	1.05	1.22	1.22	1.02	<1.07	<1.07
	Undrained (Dry)		1.22	1.22	1.12	<1.07	<1.07
	Undrained (Sat.)		1.05	1.05	1.05	1.31	1.31

Note: D10, D30, and D60 are the particle sizes for different percentage passing values, and C_u and C_c are the coefficients of uniformity and curvature, respectively.

Table 3: Comparison of the changes in the particle size distribution of dry Mason sand with different initial relative densities after drained isotropic compression to 160 MPa

Specimen	Dense	Baseline	Loose
Initial void ratio, e_0	0.51	0.57	0.61
Initial relative density, $D_{r,0}$	0.96	0.75	0.60
D_{10} (mm)	<0.075	<0.075	<0.075
D_{30} (mm)	0.14	0.14	0.14
D_{60} (mm)	0.41	0.41	0.41
C_u	<6.00	<6.00	<6.00
C_c	<1.07	<1.07	<1.07

Table 4: Comparison of the changes in Marsal's breakage factor (B_M) and Hardin's relative breakage index (B_r) for Mason sand having e_0 = 0.57 during isotropic compression with different testing conditions

Mean stress, p'(drained) or p (undrained) (MPa)	Marsal's breakage factor (B_M)			Hardin's relative breakage index (B_r)		
	Drained (Dry)	Undrained (Dry)	Undrained (Sat.)	Drained (Dry)	Undrained (Dry)	Undrained (Sat.)
10	0.04	0.03	0.00	0.02	0.01	0.00
20	0.04	0.04	0.01	0.01	0.01	0.01
40	0.08	0.07	0.02	0.07	0.06	0.00
80	0.14	0.13	0.01	0.11	0.11	0.00
160	0.19*	0.18	0.02	0.16+	0.16	0.00

*For specimens with different initial void ratios at 160 MPa: B_M=0.20 for e_0=0.51, B_M=0.19 for e_0=0.61
+For specimens with different initial void ratios at 160 MPa: B_r=0.16 for e_0=0.51, B_r=0.15 for e_0=0.61

Table 5: Parameters governing the evolution in the breakage factors B_M and B_r with increasing mean effective stress for dry sand under drained conditions

Parameter	Value
Λ_M	7.0×10^{-5}
Γ_M	0.663
Λ_r	1.2×10^{-6}
Γ_r	0.990

862 **Table 6**: Coefficients of the empirical model for the drained compression curve of dry Mason

863 sand having different initial relative densities

Initial relative density, $D_{r,0}$	Loading model parameters			Unloading model parameters		
	α	β	δ	γ	χ	η
0.96	0.25	5.0×10^{-7}	0.59	3.00	$7.0.\times10^{-6}$	5.0×10^{-9}
0.75	0.30	1.7×10^{-7}	0.70	3.30	8.0×10^{-6}	1.0×10^{-8}
0.60	0.34	2.5×10^{-8}	0.60	3.00	8.0×10^{-6}	1.0×10^{-8}

864

Figure 1

Click here to download Figure Fig 1.tif

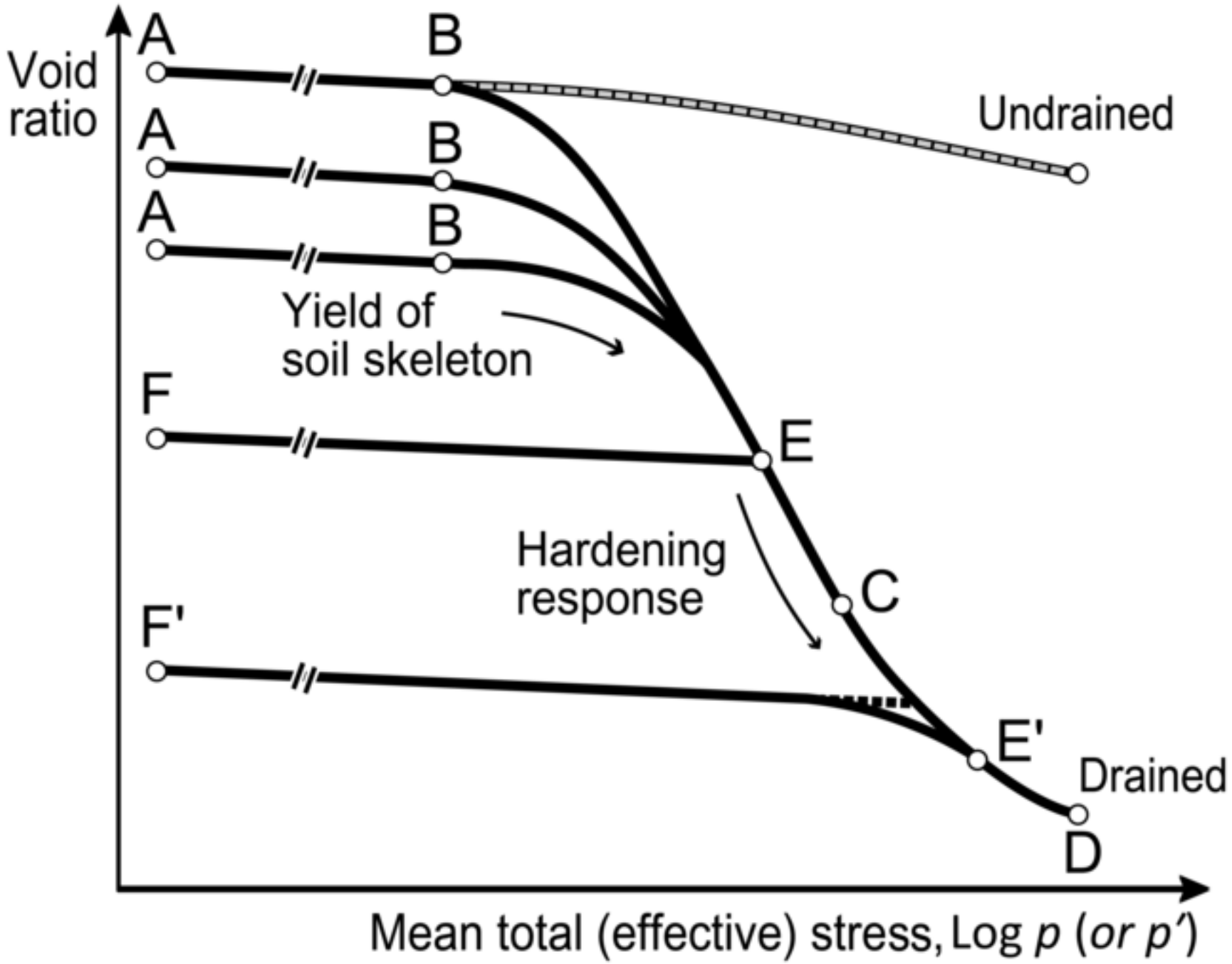

Figure 2

Click here to download Figure Fig 2.tif

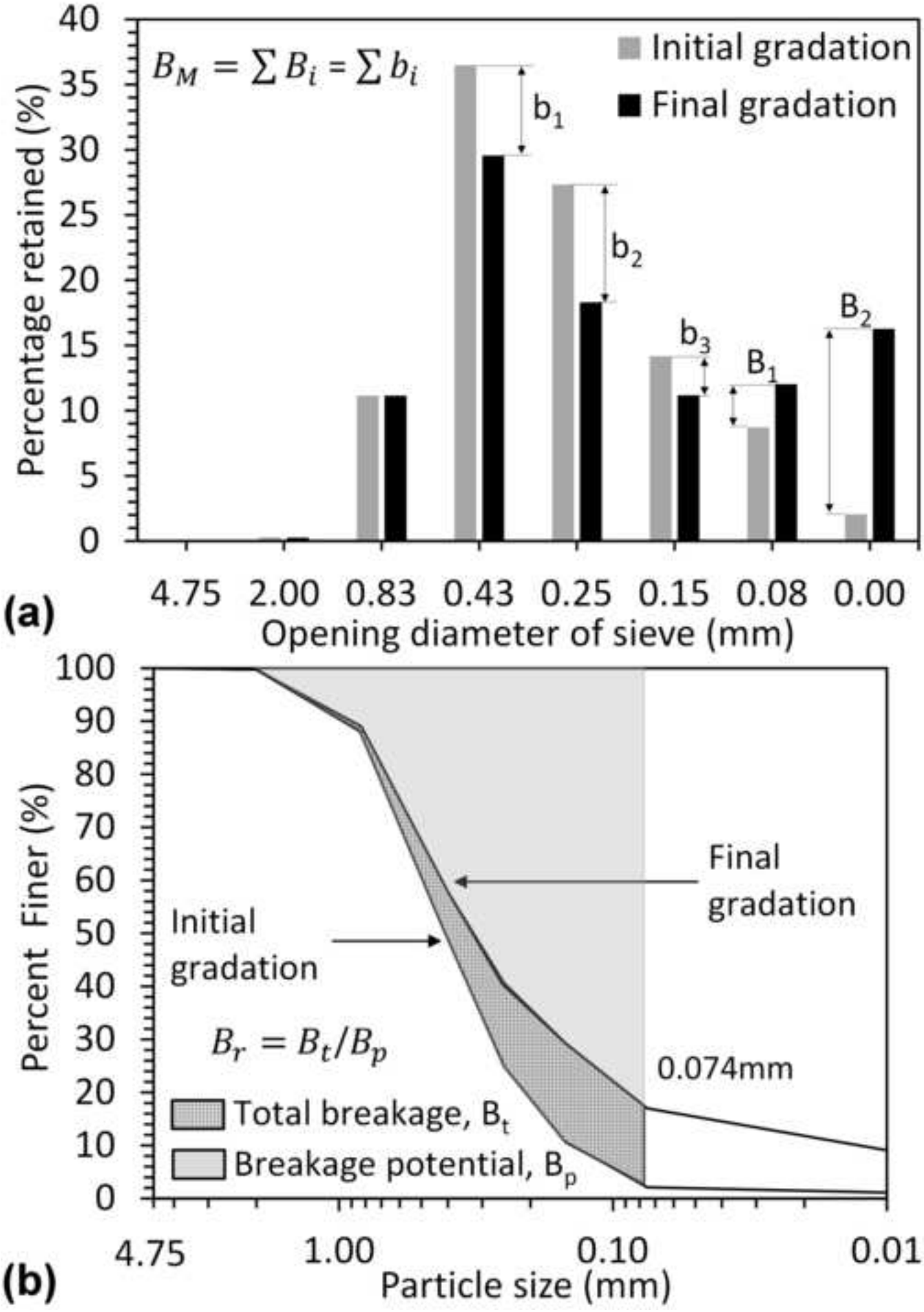

Figure 3

Click here to download Figure Fig 3.tif

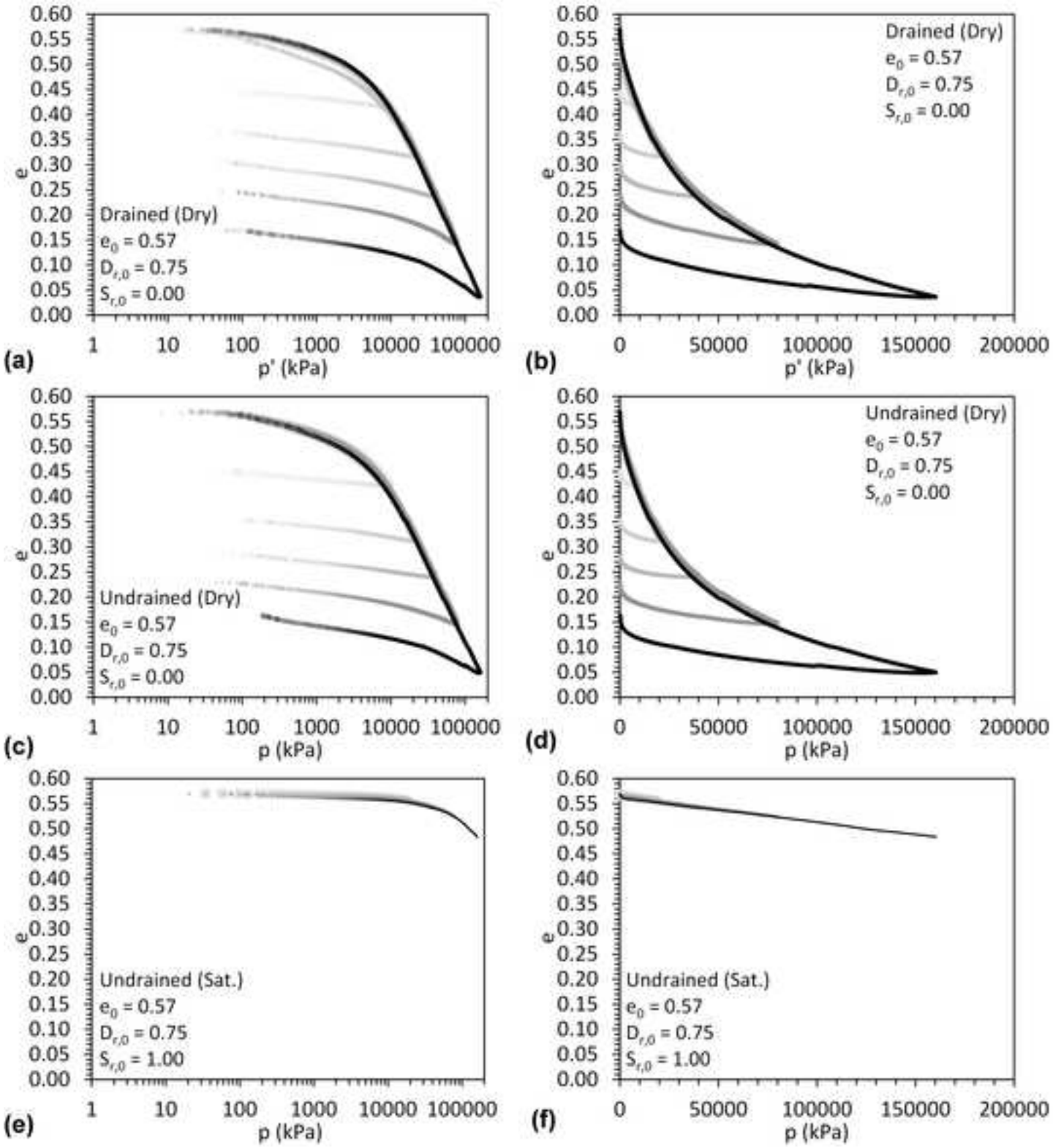

Figure 4

Click here to download Figure Fig 4.tif

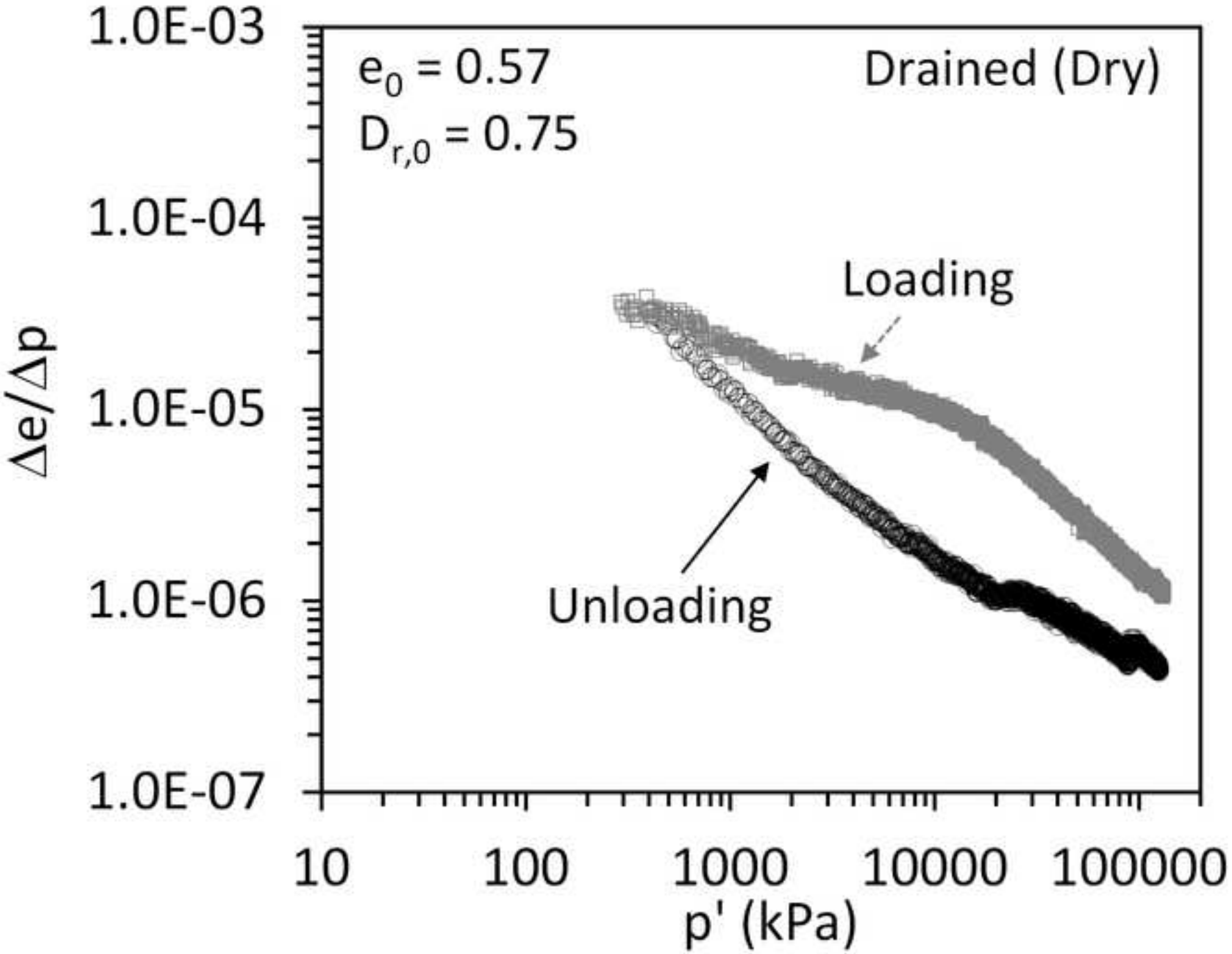

Figure 5

Click here to download Figure Fig 5.tif

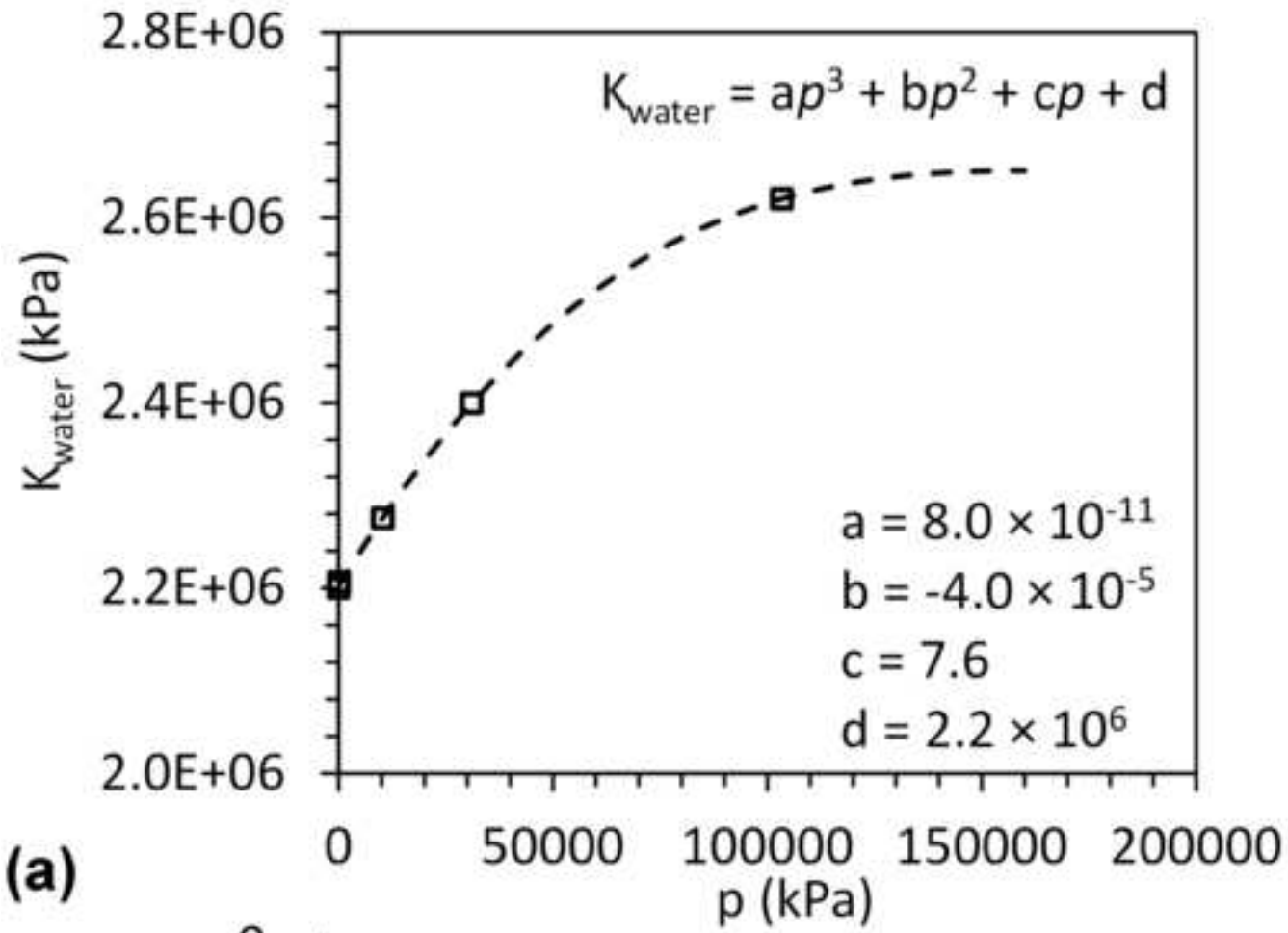

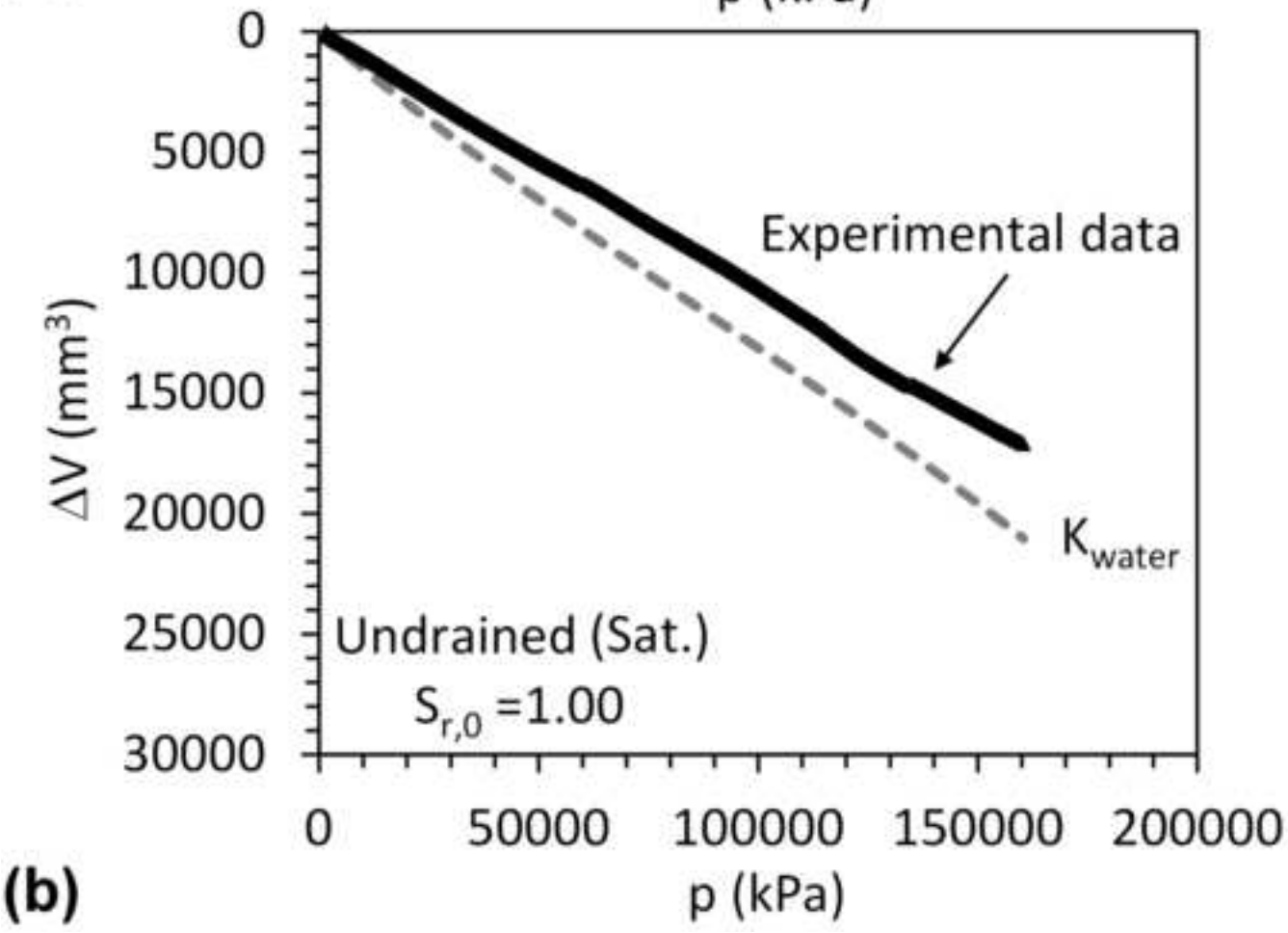

Figure 6

Click here to download Figure Fig 6.tif

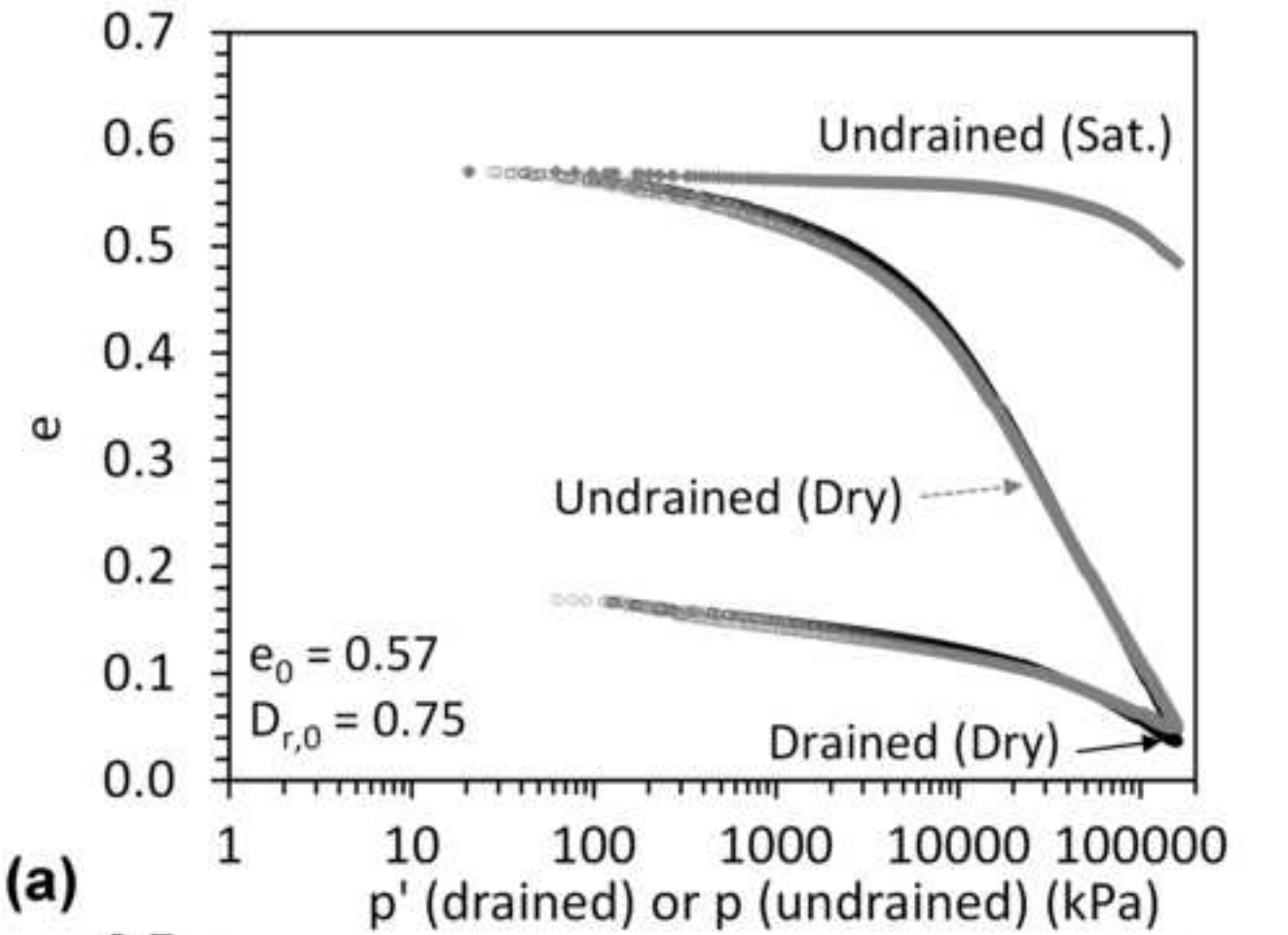

(a)

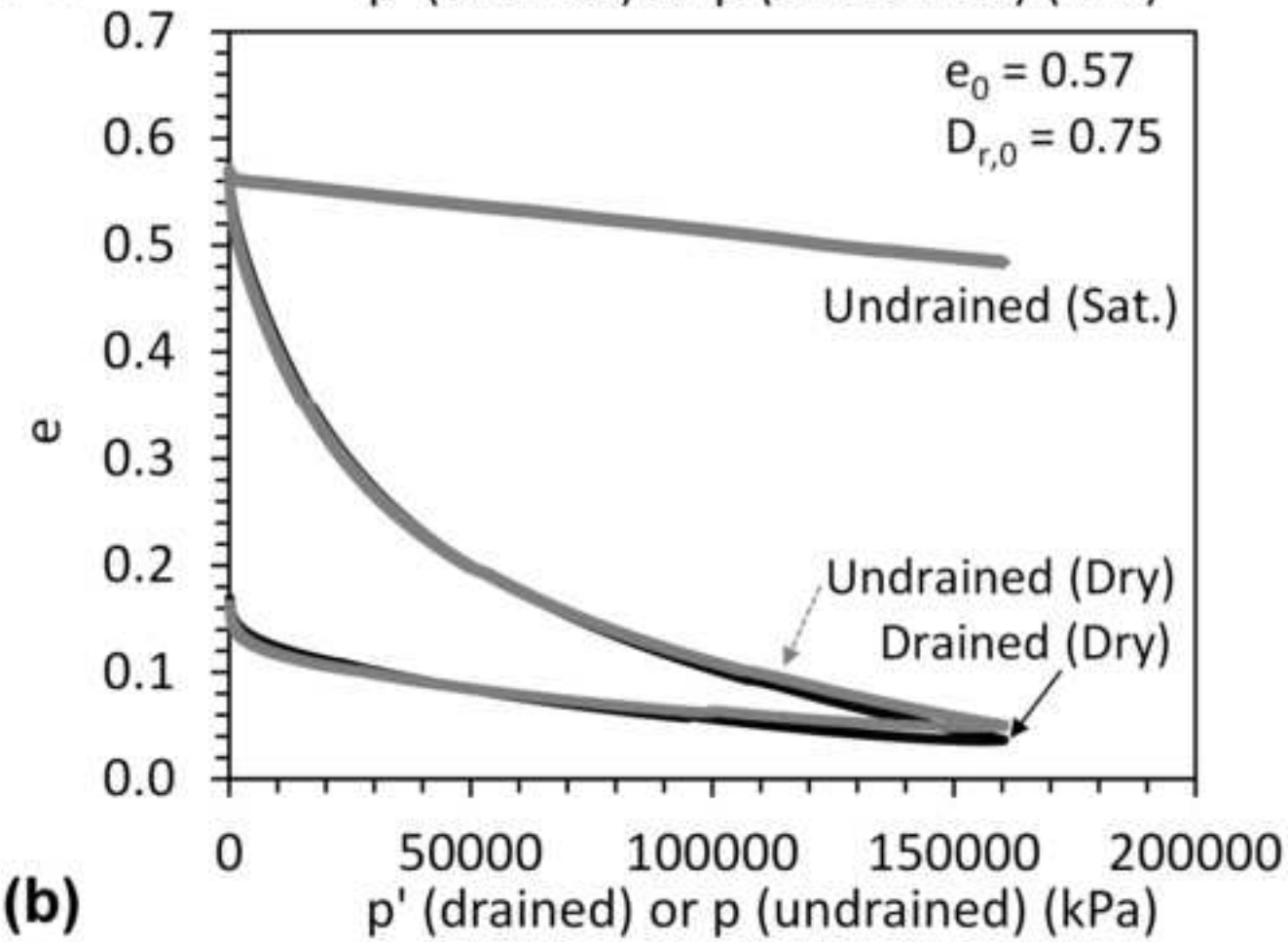

(b)

Figure 7

Click here to download Figure Fig 7.tif

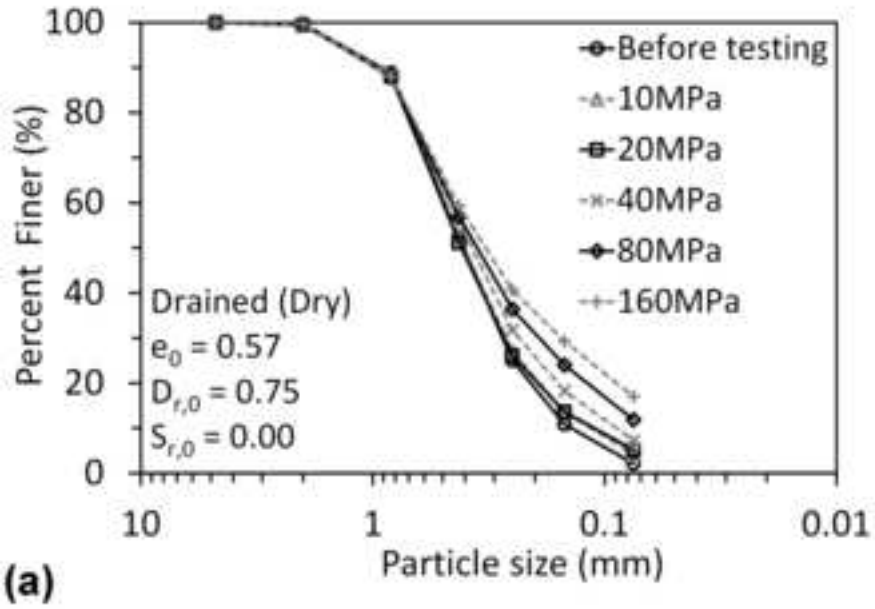

(a)

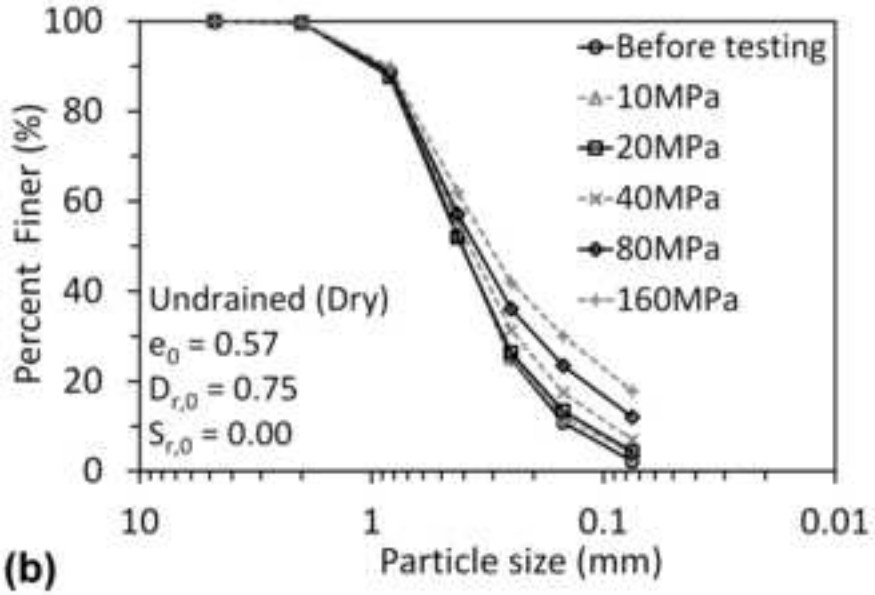

(b)

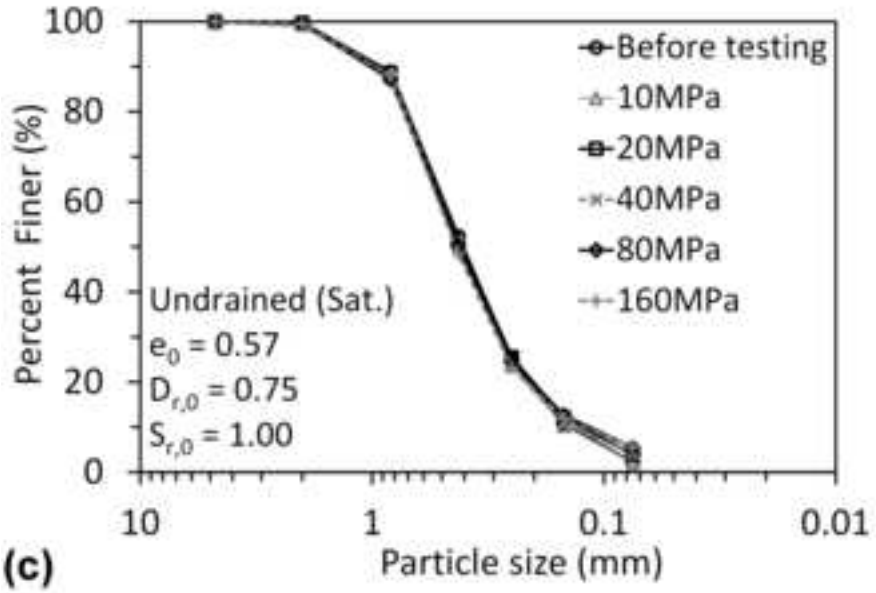

(c)

Figure 8

Click here to download Figure Fig 8.tif

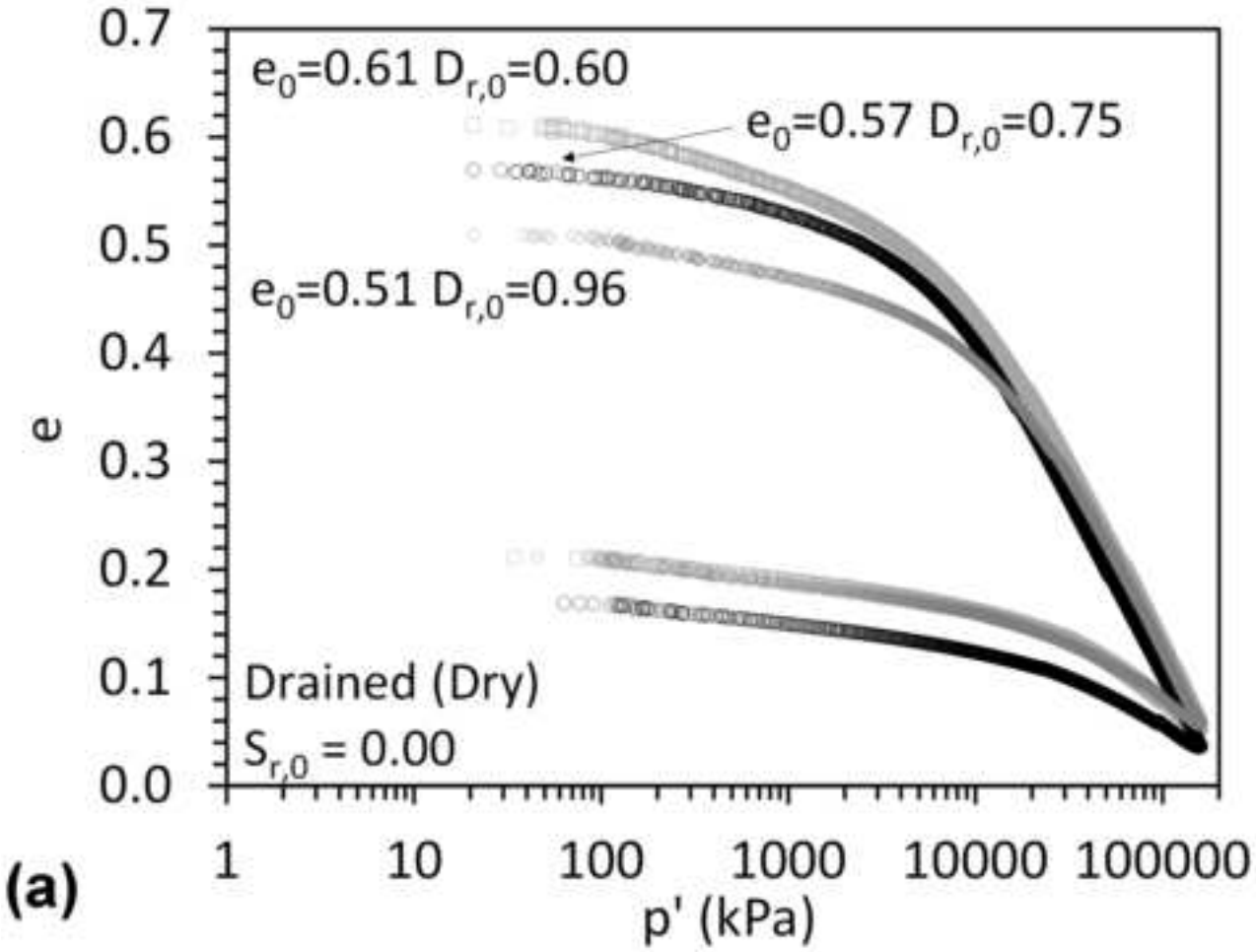

(a)

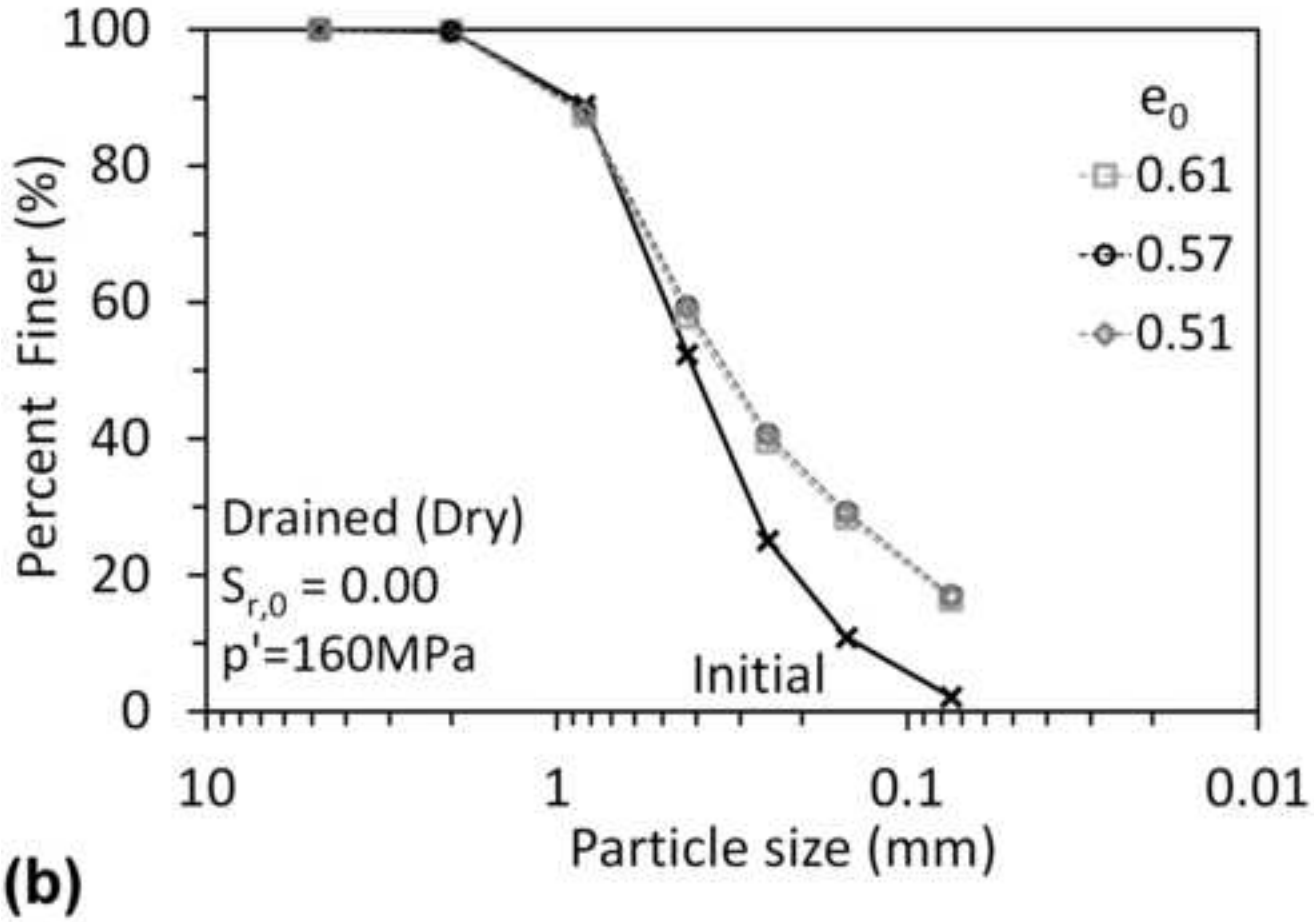

(b)

Figure 9

Click here to download Figure Fig 9 Updated.tif

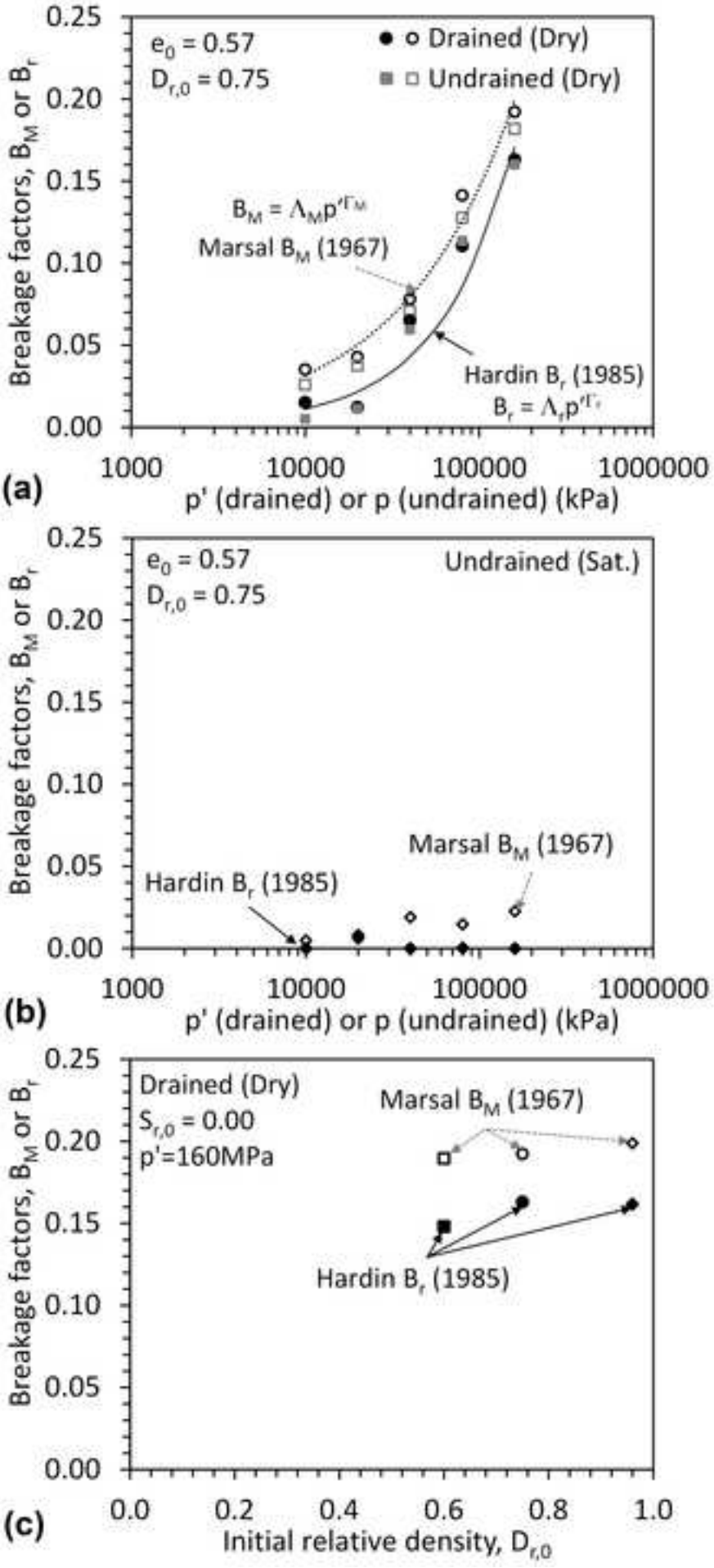

Figure 10

Click here to download Figure Fig 10.tif

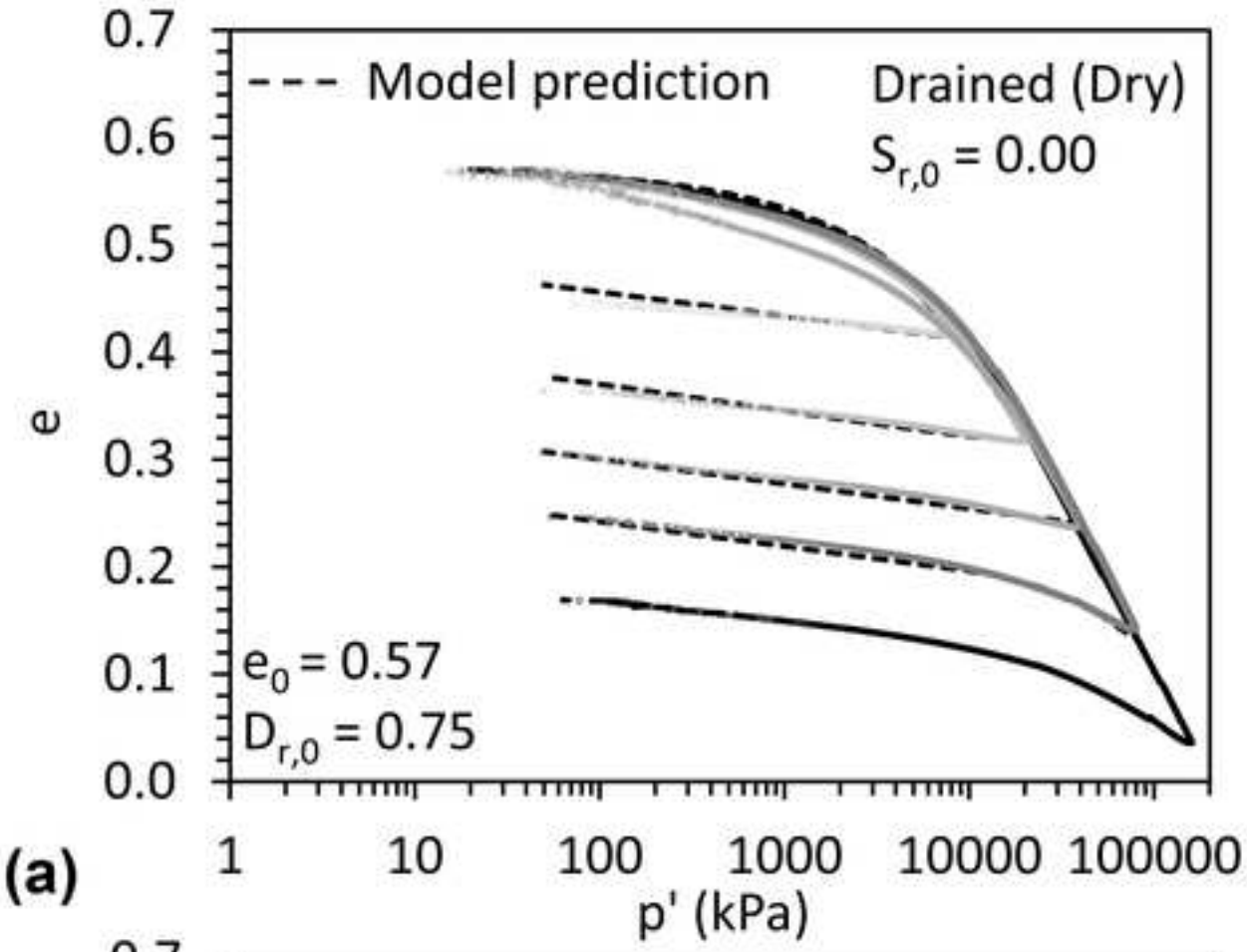

(a)

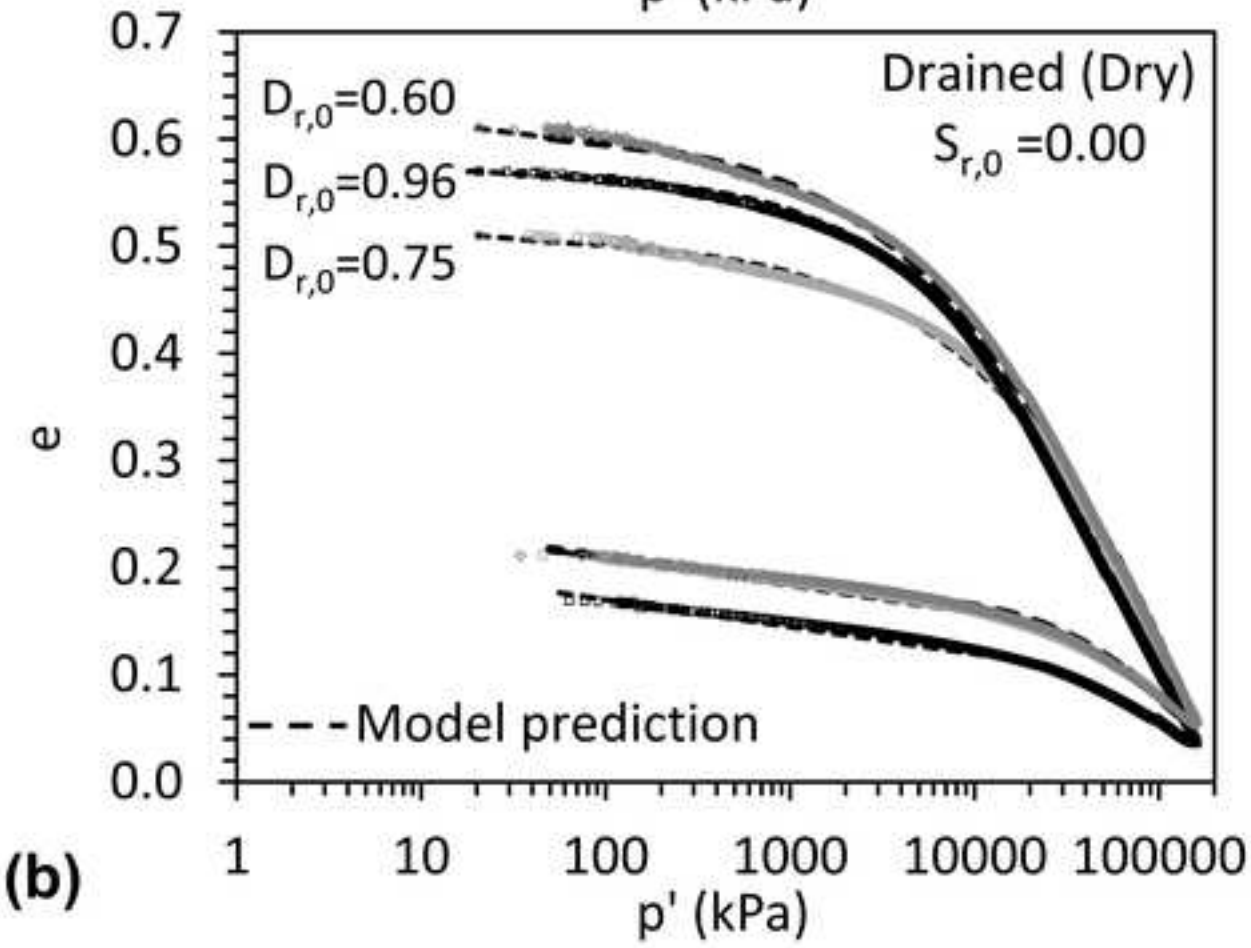

(b)